Journal of Manufacturing Processes 139 (2025) 105–125

Contents lists available at ScienceDirect

Journal of Manufacturing Processes

journal homepage: www.elsevier.com/locate/manpro

Elucidation of alkali element's role in optimizing metal transfer behavior in rutile-type flux-cored arc welding

Dang Khoi Le [a], Shinichi Tashiro [a,*], Quang Ngoc Trinh [a,b,*], Tetsuo Suga [a], Naoki Sawamura [c], Kazuhiro Fukuda [c], Shuji Sasakura [c], J. Eduardo Alvarez-Rocha [d], Patricio Fernando Mendez [d], Anthony B. Murphy [e], Van Hanh Bui [b], Manabu Tanaka [a]

[a] Joining and Welding Research Institute, Osaka University, Japan
[b] Hanoi University of Science and Technology, Viet Nam
[c] Kobe Steel, Ltd., Japan
[d] University of Alberta, Canada
[e] CSIRO, Manufacturing, Australia

ARTICLE INFO

Keywords:
Flux-cored arc welding
Sodium vapor
Metal transfer

ABSTRACT

This study investigates the effects of alkali elements on metal transfer behavior in rutile flux-cored arc welding. Four types of prototype flux-cored wires with different sodium contents in the flux were fabricated. By using these wires, the influence mechanism of sodium on the metal transfer behavior was elucidated through shadowgraph measurements of the metal transfer behavior as well as spectroscopic and color image observations of the arc characteristics. It was found that the metal transfer between 190 A and 310 A was in the projected transfer mode and could be further classified into two sub-modes (type A and type B) based on the droplet formation process. A larger droplet was formed on the side of flux column in type A, while a smaller one was formed in the center covering the flux in type B. The metal transfer frequency became larger in the latter case for the same wire feeding speed. Type A tended to dominate in the lower current and lower sodium content conditions, while type B dominated in the opposite conditions. The dominant sub-mode was determined to depend on the Lorentz force acting on the droplet. At medium currents (250 A and 280 A), both sub-modes appeared in similar proportions. The maximum metal transfer frequency occurred at a particular sodium content. When the sodium content was smaller or larger, type A or type B became dominant, respectively. The sodium content at which the maximum frequency occurred decreased when the current increased. In type A, the iron plasma was widely distributed on the droplet side of the flux, while the sodium plasma was concentrated near the flux on the opposite side, so both were separated. In contrast, in type B, the sodium plasma was concentrated around the flux at the center and the iron plasma was widely distributed in the arc column, so both overlapped around the center. Sodium has a low boiling point and low ionization potential. In type A, the sodium vapor greatly increased the electrical conductivity of plasma around the flux column, so part of the current flowed from the wire through the sodium plasma to the weld pool. Accordingly, the current flowing through the bottom of the droplet to the arc decreased, leading to a lower arc pressure and recoil pressure under the droplet, and causing the metal transfer frequency to increase with sodium content. On the other hand, in type B, the sodium vaporization increased around the center, increasing the recoil pressure. In addition, the current density at the bottom of the droplet increased due to the current concentration in the arc, causing the arc pressure to rise. Therefore, the metal transfer frequency tended to decrease with sodium content. Due to the balance of these factors, the metal transfer frequency has a maximum at a particular sodium content.

1. Introduction

Gas Metal Arc Welding (GMAW), in which a consumable wire electrode is continuously fed and melted due to the heat input from an arc to fill a gap between plates, is the most commonly used arc welding process [1]. In GMAW, two kinds of electrodes are generally used: a solid

* Corresponding authors.
E-mail addresses: tashiro.shinichi.jwri@osaka-u.ac.jp (S. Tashiro), ngoc.trinhquang@hust.edu.vn (Q.N. Trinh).

https://doi.org/10.1016/j.jmapro.2025.02.021
Received 5 November 2024; Received in revised form 30 January 2025; Accepted 10 February 2025
Available online 17 February 2025

wire and a tubular wire. The latter process uses a flux incorporated in the wire, so-called Flux-Cored Arc Welding (FCAW), which provides a high deposition rate leading to high welding speed, high welding stability, applicability to various welding positions and so on depending on the flux composition [2]. Owing to these benefits, FCAW has been studied by many researchers for a long time and currently has various applications in industry [3]. FCAW can be categorized into two types depending on the shielding method; one uses an external shielding gas, and the other uses the vaporized flux from the wire to protect the welding area. In the former case, the tubular wire has a concentric double structure consisting of an inner flux and an outer metal sheath. This process is further classified into sub-groups according to the flux composition as Metal-Cored Arc Welding (MCAW) [4], basic-type FCAW [5] and rutile-type FCAW [6].

In GMAW, including FCAW, understanding and control of the metal transfer process are important for improving the efficiency and final quality of the weld bead, because a large part of heat input to the weld pool is carried by the high-temperature droplet detached from the wire [7]. For example, Soderstrom et al. measured an average droplet temperature in the free-flight mode of GMAW for ER70S-6 (carbon steel), ER316L (stainless steel), and ER4030 (aluminum alloy) electrodes. The results showed that the droplet temperature increased to much than the melting point of the wire material and reached around its boiling point, particularly in cases of ER70S-6 and ER4030 [8]. The metal transfer mode in GMAW changes depending on various factors [9–11]. When using a solid wire, the mode transitions to short-circuiting, drop (globular), spray and then streaming as the current increases as categorized by the International Institute of Welding (IIW) [12]. Numerous investigations were conducted to clarify the metal transfer behavior in GMAW using a solid wire. In particular, because of their importance, many researchers have reported the effects of the welding current and shielding gas composition on the metal transfer mode. Ushio et al. showed experimentally that the transition current from the globular mode to spray mode increased with CO_2 content in the Ar-CO_2 shielding gas by >10 % due to an increase in arc pressure under the droplet [13]. Taking advantage of recent progress in computational modeling, the metal transfer process in GMAW can be investigated considering the various driving forces acting on the droplet [14]. Ogino et al. clarified the above mechanism governing the transition current systematically by using numerical simulation [15]. Liu et al. studied the variation in the metal transfer mode and frequency, reporting the optimum condition under which the maximum metal transfer frequency was achieved [16]. Hu and Tsai investigated a series of phenomena in the metal transfer process, including electrode melting, the formation, detachment, and transfer of droplets, and then the droplet impingement onto the workpiece via numerical simulation considering the temperature and flow fields inside the droplet [17]. Kim and Eagar predicted the droplet size based on both the static force balance theory and the pinch instability theory as a function of welding current [18]. They reported that the metal transfer with steel electrodes shielded with Ar-2 % O_2 showed a gradual transition from globular to projected spray, followed by the streaming transfer mode.

Unlike the solid wire, the tubular wire contains an inner flux consisting of metal and/or oxide components with low electrical conductivity. As a result, the current path in the tubular wire exhibits quite different behaviors, primarily flowing through the outer metal sheath and avoiding the inner flux. This decisively affects the metal transfer process.

MCAW has the simplest flux composition in FCAW processes because it mainly consists of metal elements. Therefore, the metal transfer process in MCAW has been investigated more deeply than those in other types of FCAW. Starling and Modenesi compared the metal transfer behavior in MCAW, basic-type FCAW and rutile-type FCAW in different shielding gas compositions observed by a shadowgraph method [19]. Trinh et al. studied the effects of CO_2 content in the argon-CO_2 shielding gas on the metal transfer frequency [20]. The peak of metal transfer frequency appeared at 15 % CO_2 in the current range from 220 A to 280 A. The results indicated that the relationship between the positions of the arc attachment and the tip of the un-melted flux column strongly affected the metal transfer behavior. The smaller CO_2 content makes the arc attachment position higher than that of the un-melted flux, causing the Lorentz force to be ineffective in droplet detachment, while the larger content increases the arc pressure under the droplet to prevent droplet detachment. Accordingly, the above balance produces the peak of frequency. Tashiro et al. studied the droplet detachment process with numerical simulation [21]. They found that when the arc attachment position was higher than that of the un-melted flux location, the current conduction through the droplet was greatly decreased, making the Lorentz force inside the droplet negligibly small. Therefore, an eddy containing upward flow at the central axis was induced inside the droplet, preventing neck formation. In contrast, when the arc attachment position became lower, the eddy disappeared, and a unidirectional downward flow formed inside the droplet to start the neck formation.

Furthermore, in recent studies, the addition of very small amounts of alkali elements into the flux has been found to decisively govern the metal transfer process in MCAW. Valensi et al. found that the addition of an alkali element stabilized the metal transfer, keeping the spray transfer mode up to 60 % CO_2 in Ar-CO_2 shielding gas at 330 A [22]. Following this, Trinh et al. also investigated the effect of alkali elements on the metal transfer behavior in Ar-20%CO_2 shielding gas in more detail [23]. They found that when increasing the sodium content in the flux, the metal transfer frequency increased thanks to the formation of a direct current path from the wire tip to the weld pool through the sodium plasma bypassing the droplet, thus reducing the current flowing through the iron plasma under the bottom of the droplet to decrease the arc pressure acting on the droplet. This was a consequence of the low boiling point and low ionization potential of sodium. Bui et al. investigated the effect of sodium in the flux on the metal transfer behavior in pure argon shielding gas at 280 A and 320 A, corresponding to the current range for projected and streaming transfers, by comparing the results with the solid wire case [24]. They revealed that even at the current for the streaming transfer in the solid wire case, the metal transfer mode was kept to the projected transfer in MCAW because the sodium vapor was mixed into the metal plasma under the droplet, increasing the electrical conductivity of the plasma. As described above, the effect of alkali elements is also predicted to be important in other types of FCAW.

From the above research results for MCAW, it can be inferred that the effects of the un-melted flux, as well as the additional alkali elements in the flux, will also play important roles in the metal transfer behavior in rutile-type FCAW. Regarding the former, the un-melted flux region tends to be longer than that in MCAW. The formation mechanism of molten droplets is known to be strongly affected by the presence of the long flux column, making understanding the metal transfer more complicated [25]. While the metal transfer modes in rutile-type FCAW were summarized as functions of current and shielding gas composition by Izutani et al. [26], the underlying metal transfer mechanisms are not yet well understood.

Matsuda et al. studied the effects of iron powder ratio in the flux on droplet size, reporting that the droplet size decreased with decreasing the flux column length. This length decreased with an increase in the iron powder ratio. [27]. Trinh et al. investigated the effects of CO_2 content in Ar-CO_2 shielding gas on metal transfer behavior in rutile FCAW [28]. Similar to the result in MCAW [20], a peak frequency appeared at a particular content, but the CO_2 content for the peak frequency decreased with increasing current. The result indicated that the metal transfer can be optimized by shortening the length of un-melted flux, which can be done by decreasing the CO_2 content in Ar-CO_2 shielding gas or increasing the welding current. Regarding the latter, the arc characteristics in FCAW are well known to be complicated by the mixing of the highly vaporized alkali element into the plasma. Because of this mixing, the thermodynamic and transport properties of plasma

are dramatically changed mainly due to the low ionization potential of alkali element, strongly affecting the current path in the arc, which governs the heat and force balances between the arc and wire as well as the metal transfer behavior. Although there are various works studying rutile-type FCAW, our survey indicates that research results clarifying the effect of alkali elements on the metal transfer behavior based on detailed observations such as spectroscopic measurements are lacking. In addition, Suga et al. reported that the addition of flux compounds with high vapor pressure, such as CaF_2, delayed the droplet detachment due to an increase in the recoil pressure acting on the bottom of the droplet caused by the vaporization [29]. Therefore, the recoil pressure due to the vaporization of alkali elements is also predicted to be important.

This study aims to investigate the effects of alkali elements on metal transfer behavior in rutile-type FCAW. Among the six alkali metals, sodium and potassium are suitable for use as industrial products in terms of price and availability. Especially, sodium has the advantage of being less susceptible to moisture absorption when added, so sodium was chosen as the alkaline element. In this study, four types of prototype flux-cored wires with different sodium contents in the flux were fabricated. By using these wires, the mechanisms by which sodium affects the metal transfer behavior are elucidated through shadowgraph measurements of the metal transfer behavior as well as spectroscopic and color image observation of the arc characteristics.

2. Experimental methodology

2.1. Welding conditions and materials

The bead-on-plate welding experiments for FCAW were carried out using mild steel plates (SS400 – JIS G 3101) with a dimension of 300 mm × 50 mm × 9 mm. Four types of prototype flux-cored wires with a diameter of 1.2 mm and classified under AWS A5.20 E70T-1C were employed. The sodium content in these wires varied from 0 % to 0.12 % in increments of 0.04 %. Specifically, the wires consisted of wire 1 (no sodium), wire 2 (0.04 % sodium), wire 3 (0.08 % sodium), and wire 4 (0.12 % sodium). The sodium is useful as an arc stabilizer, but adding a large amount of sodium is thought to cause the flux to absorb moisture and also increase fume. Therefore, the range of sodium content was determined considering the above factors. The sodium was added to the flux as a compound, which was expected to be thermally decomposed to Na_2O when the wire temperature increased. Na could then be produced by thermal decomposition due to further increase in temperature or reduction through chemical reactions with other compounds such as silicon oxide and manganese oxide. The chemical composition of the wires is detailed in Table 1. The chemical compositions other than sodium are almost identical for all the wires.

The welding power source (DP-350, OTC Daihen) paired with a wire feeder was operated in a Direct Current Electrode Positive (DCEP) mode. The welding torch was set with a Contact Tip to Workpiece Distance (CTWD) of 20 mm, and the initial distance from the wire tip to the plate surface before starting each experiment was 10 mm. The welding speed was 5 mm per second. To examine the impact of alkali elements on metal transfer and arc behavior, a series of experiments was conducted at five currents: 190 A, 220 A, 250 A, 280 A, and 310 A. The arc voltage was adjusted between 30.0 V and 34.5 V to keep the arc length constant as possible. An Ar-20 % CO_2 mixture was used as the shielding gas, with a flow rate of 20 L/min. The welding conditions are listed in Table 2.

Table 1
Chemical compositions of the prototype wires (mass%).

Wire no.	C	Si	Mn	Ti	Na	Fe
1	0.05	1.00	2.53	3.37	0	89.3
2	0.05	1.00	2.53	3.37	0.04	89.3
3	0.05	0.99	2.53	3.37	0.08	89.2
4	0.05	0.99	2.53	3.37	0.12	89.2

2.2. Metal transfer observation

The metal transfer behavior was observed by the shadowgraph method, using a high-speed video camera (HSVC) (Memrecam Q1v, Nac Image Technology), a 640-nm wavelength laser illumination system (Cavilux HF system, Cavitar), and an object lens (Micro-NIKKOR, Nikon) with a 200 mm focal length and a 1/4 focus ratio. The observation was conducted at 4000 fps, with an aperture of f/8 and an exposure time of 20 μs. To minimize arc radiation, five Neutral-Density (ND) filters, including four ND-8 filters and one ND-4 filter, were used. When applying the shadowgraph method, a bandpass filter for the same wavelength with the laser illumination system is generally employed to eliminate the arc radiation as possible. However, in this study, only ND filters were attached to HSVC without using the bandpass filter to observe the metal transfer behavior and arc appearance at the same time. Fig. 1 illustrates the experimental setup for observing the metal transfer behavior.

2.3. Arc phenomena observation

Two types of experiments were carried out to analyze the arc phenomena. Fig. 2 shows the setup for the first type of experiment for observing the three line spectrums of iron, argon, and sodium atoms independently using a monochrome HSVC (Memrecam Q1v, Nac Image Technology) with band-pass filters. The frame rate was 4000 fps. The welding voltage and welding current waveforms were also recorded through a data logger system (NR-500/NR-HV04, Keyence) connecting to the clamp meter (3285, HIOKI), which was synchronized with the HSVC for its triggering. An additional voltage power source of DC 5 V was used for detecting the starting moment of the main arc. Three types of band-pass filters with a Full Width at Half Maximum (FWHM) of 10.0 nm and central wavelengths of 540.0 nm (Fe I), 694.0 nm (Ar I), and 589.0 nm (Na I) were used for observing the behavior of each element in the plasma. The detail of arc phenomena observation using bandpass filters was the same as that described in [23]. The camera settings were consistent with those used in the shadowgraph method, which included three ND-8 filters.

Since this method only allowed for individual observation of the line spectrum for the iron, argon, and sodium atoms, it could not be used for comparing the plasma behaviors of different elements at the same time. To address this limitation, a second type of experiment was carried out using a color HSVC (Memrecam ACS-1, Nac Image Technology) with the same objective lens as used in metal transfer behavior studies, but with an aperture of f/22. Fig. 3 shows the details of the experimental setup, which enables simultaneous observations of the arc phenomena of different elements according to the color of the plasma radiation. The color camera was operated at a frame rate of 75,000 fps with an exposure time of 12 μs, and four ND filters (three ND-8 and one ND-4) were used to reduce the arc radiation.

Table 2
Welding conditions.

Welding parameters	Value
Welding current	190 A, 220 A, 250 A, 280 A and 310 A
Arc voltage	30.0 V–34.5 V
Welding velocity	5 mm/s
CTWD	20 mm
Shielding gas	Ar – 20 % CO_2; 20 L/min

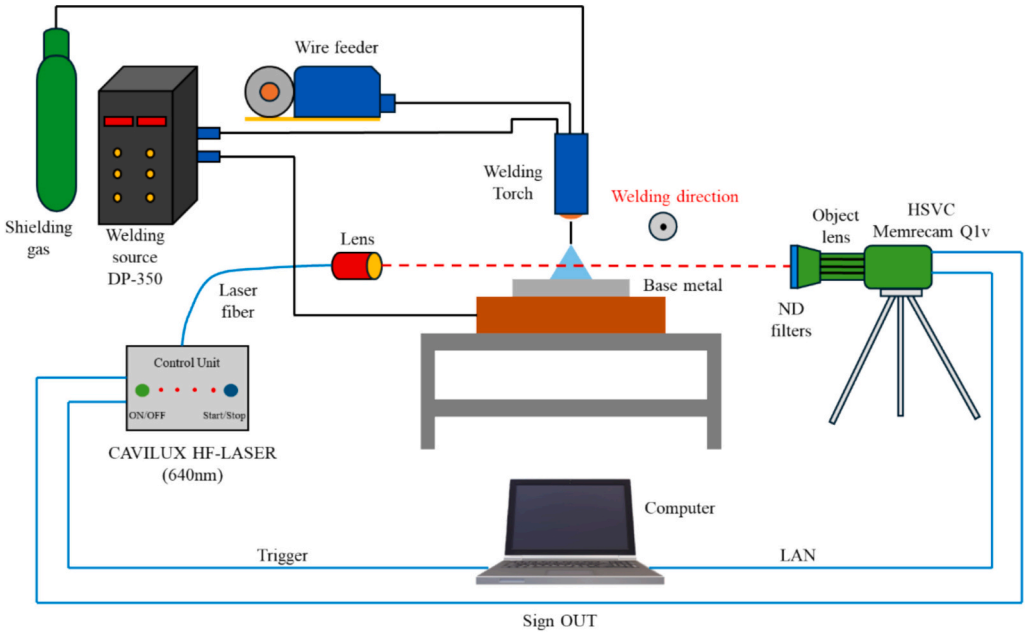

Fig. 1. Schematic of experimental setup for observing the metal transfer behavior using shadowgraph method.

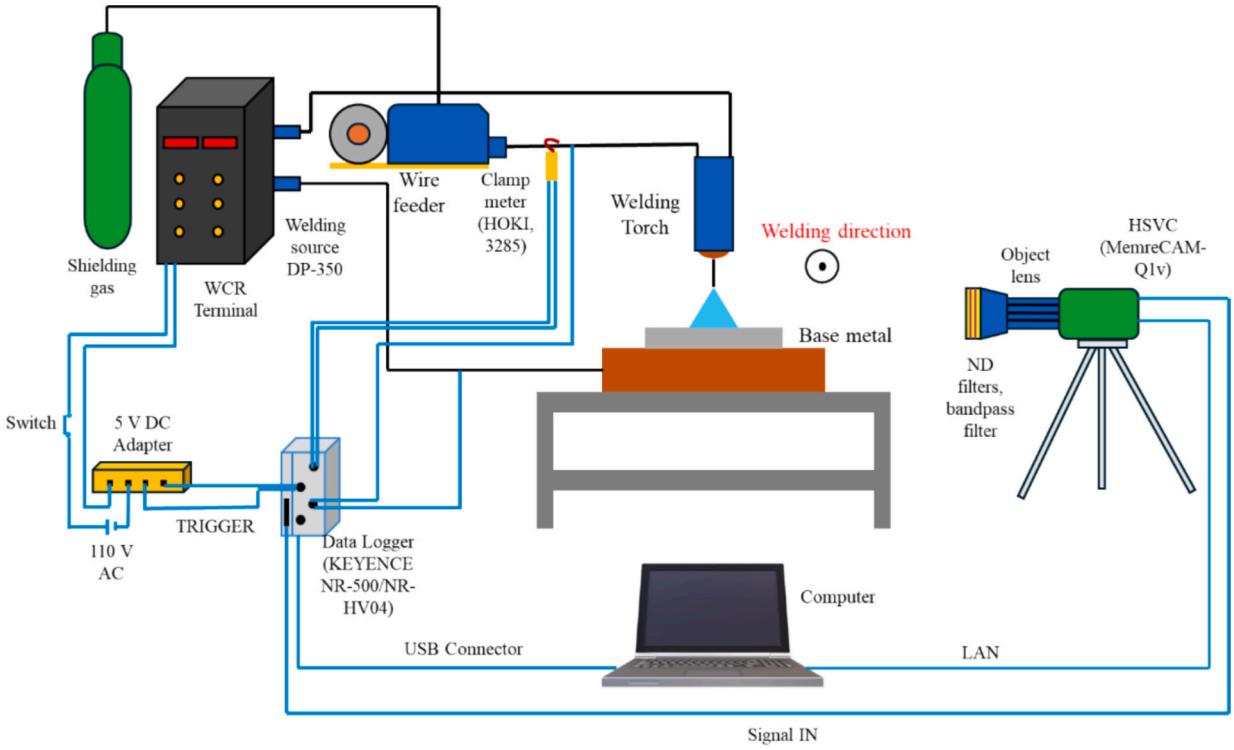

Fig. 2. Schematic of arc phenomena observation setup using a high-speed camera equipped with band-pass filters and a data logger for measuring current and voltage waveforms.

3. Results and discussion

3.1. Metal transfer behavior

Fig. 4 shows the metal transfer frequency for the four prototype wires as a function of sodium content at five welding currents. Using the same method as in [28], ten random durations of 250 milliseconds were selected to count the number of droplets, and then the frequency of each duration was calculated by dividing the number of droplets by the time elapsed from the first to the last detachment. After that, a final frequency was determined as an average value of these ten frequencies, while the error bars depicted the standard deviation. In this analysis, only droplets consisting of molten metal were counted, ignoring the detached flux.

As presented in Fig. 4, with all the examined flux-cored wires, the higher the welding current, the greater the metal transfer frequency. The increase in welding current enhanced the melting rate of the metal sheath, leading to a higher metal transfer frequency. Except for the lowest welding current of 190 A with almost constant frequencies of

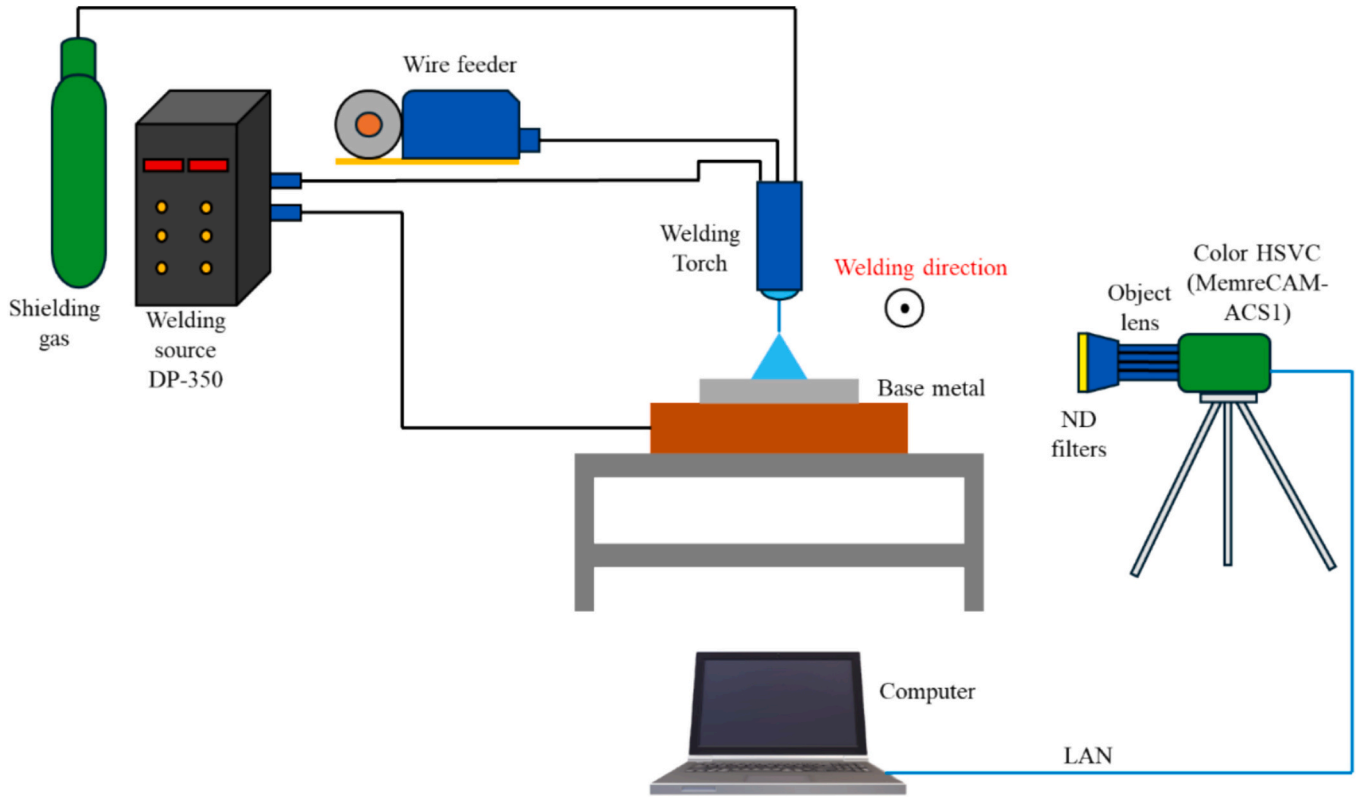

Fig. 3. Schematic of arc phenomena observation setup using a color high-speed camera.

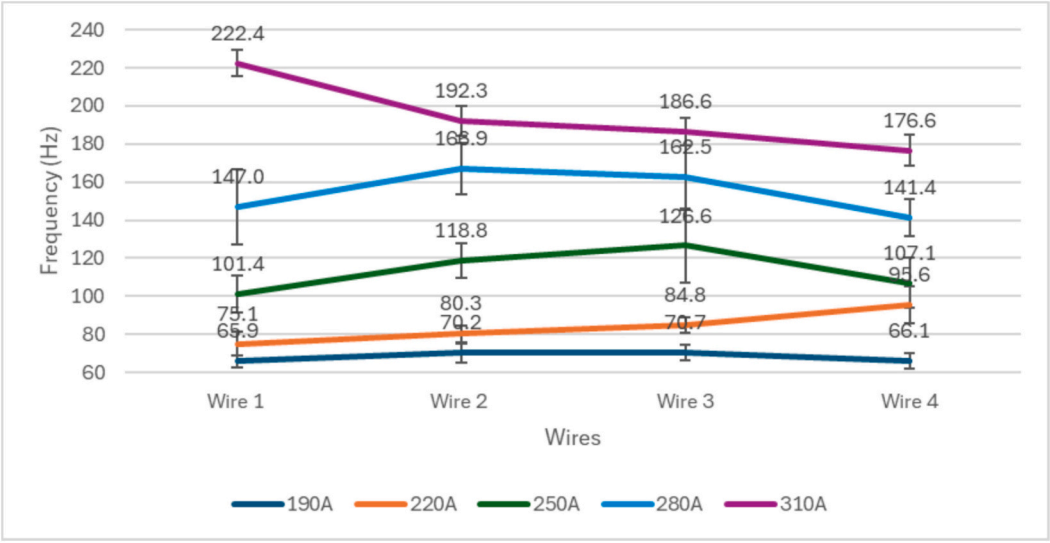

Fig. 4. Metal transfer frequency as a function of sodium content at five welding currents.

65.9 Hz, 70.2 Hz, 70.7 Hz and 66.1 Hz in wire 1, wire 2, wire 3 and wire 4, respectively, the frequency attained a maximum value as a function of sodium content. At the medium-low welding current of 220 A, the frequency increased gradually from 75.1 Hz to 95.6 Hz with an increase in the sodium content. At the medium welding current of 250 A, the metal transfer frequency increased from 101.4 Hz to 126.6 Hz as the sodium content increased from 0 % to 0.08 % and then dropped to 107.1 Hz at 0.12 %. At the medium-high welding current of 280 A, the metal transfer frequency was 147.0 Hz at 0 % sodium and increased to 166.9 Hz a 0.04 %, was almost unchanged with a frequency of 162.5 Hz at 0.08 %, and finally reduced to 141.4 Hz at 0.12 %. At the highest welding current of 310 A, the metal transfer frequency suddenly decreased from 222.4 Hz at 0 % to 192.3 Hz at 0.04 % sodium and then gradually decreased from 192.3 Hz at 0.04 % to 176.6 Hz at 0.12 %. As a result, it was found that when the welding current increased, the sodium content at which the maximum frequency appeared gradually decreased from 0.12 % to 0 % in the current range between 190 A and 310 A. The result implies that the metal transfer is significantly affected by the evaporation of sodium added to the flux.

Fig. 5 shows typical images of metal transfer behavior for different sodium contents at welding current of 190 A, 250 A and 310 A. At all the welding currents, the flux column was always formed during the

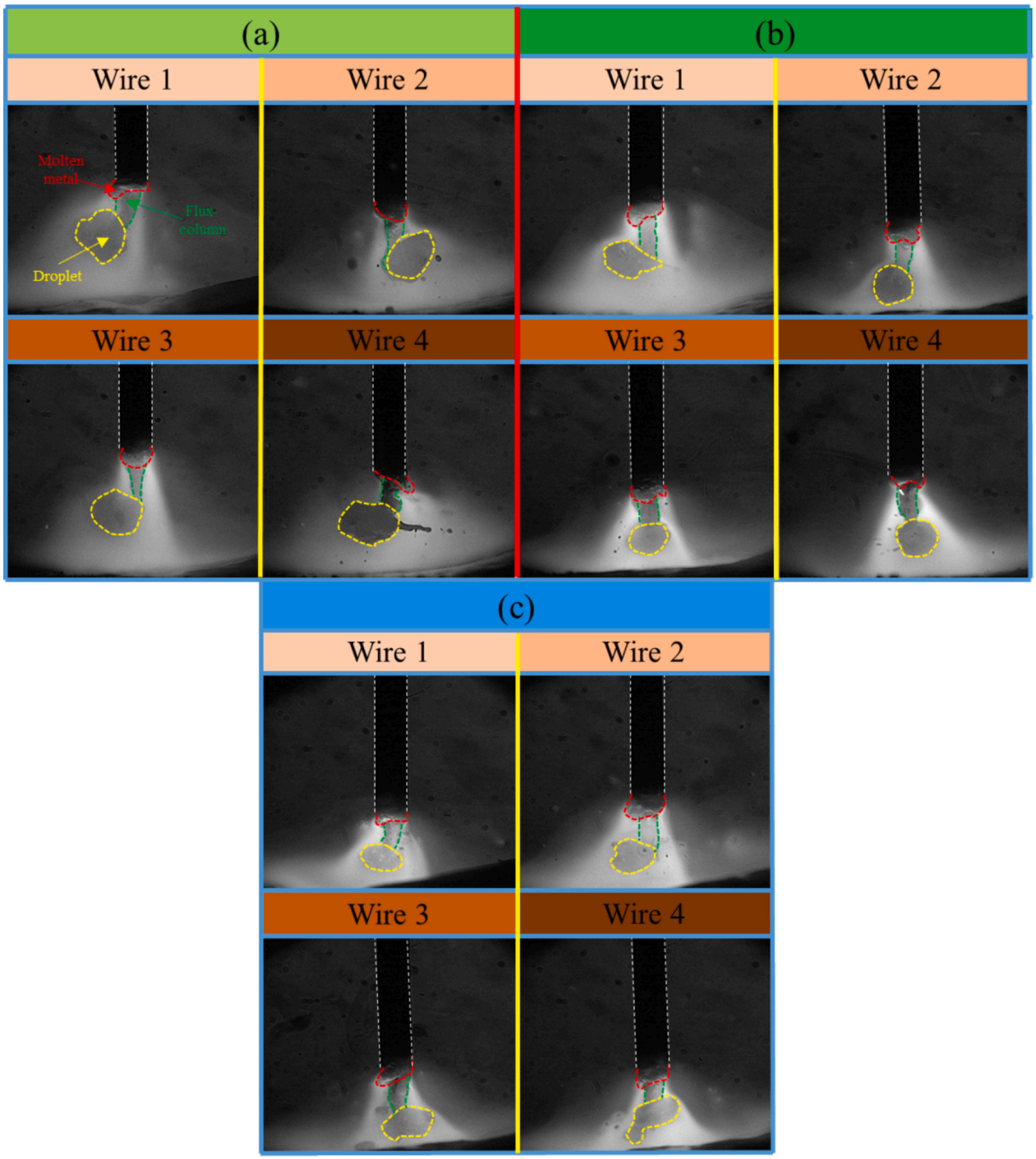

Fig. 5. Typical images of metal transfer behavior for different sodium contents at welding current of (a) 190 A, (b) 250 A and (c) 310 A.

detachment process, which is a well-known characteristic of FCAW [28]. The length of the flux column tended to increase as a function of the welding current, so the lower end of the flux column was extended further and continuously fell onto the weld pool, especially at 250 A and 310 A. The molten droplet was consistently separated from the tip of the flux column after flowing downward either along the side or through the central axis of the flux. When the welding current increased, the position of droplet formation gradually moved from the side of the wire to the central region. The droplet size was consistent with the molten metal volume estimated from the metal transfer frequency at these welding currents. In particular, the droplet diameter didn't change significantly at a welding current of 190 A, as presented in Fig. 5a. The flux column, in this case, was quite short and covered by molten metal during droplet formation. As presented in Fig. 4, the frequency rose as sodium content increased from 0 % to reach a maximum at 0.08 % and then decreased until the sodium content of 0.12 % at 250 A. Accordingly, the observed droplet size in Fig. 5b was minimum at 0.08 %. The lower end of the flux column tended to be detached independently from the metal part several milliseconds before the metal droplet detachment because this portion was melted by the intensive heat input from the arc and exposed to external forces such as the arc pressure and plasma shear force. At the welding current of 310 A, the droplet size gradually increased with increasing sodium content, as shown in Fig. 5c. The tip of the flux column was detached almost together with the molten metal, resulting in

the mixture of molten metal and flux in the droplet. Due to the elongation of the flux column, the distance between its tip and the weld pool was generally shortened. When the molten metal was mixed with the tip of the flux column, part of the droplet was sometimes dipped into the weld pool before detachment.

Similarly to GMAW using a solid wire, a transition of the metal transfer mode occurs in FCAW according to changes in the welding current. For example, Izutani et at. classified the metal transfer mode in the rutile FCAW using Ar-CO_2 mixture shielding gas as short-circuiting transfer, drop (globular) transfer, projected transfer, and streaming transfer as a function of current [26]. The projected transfer mode includes two sub-modes, as explained below. In the current range used in this paper, only the projected transfer mode was observed. In Fig. 4, the errors at the welding currents of 250 A and 280 A were seen to be much larger than those at other welding currents. These error bars are used to express the standard deviation of the frequency. This phenomenon is thought to occur because this welding current range corresponds to a transition threshold between two different metal transfer modes. According to the above classification, both the sub-modes were found to appear at 250 A and 280 A.

Fig. 6 shows a classification of two sub-modes in the projected transfer mode. These sub-modes are termed “type A” and “type B”. A larger droplet was formed on the side of the flux column in type A, while a smaller one was formed in the center, covering the flux, in type B. Under the same wire feeding speed, a larger droplet indicates a lower metal transfer frequency. Therefore, the metal transfer frequency was larger in type B. Which of the sub-modes was dominant depended mainly on the current, but the sodium content in the flux also affected it, as explained in the next section. Type A and type B were dominant at the lower currents (190 A and 220 A) and higher current (310 A), respectively.

Fig. 7 shows the time of droplet detachment in three separate periods, colored in orange, green, and blue, for wire 3 at welding currents of 250 A and 280 A. The figure allows analysis of the large errors seen in Fig. 4. The three periods were taken from the ten periods used to calculate the metal transfer frequency under each condition. The droplet detachment period was seen to be longer in the type A transfer mode, while it was shorter in type B, as explained in the previous paragraph. The result indicates that the type A metal transfer mode accounted for 68 % of the total detachments at a welding current of 250 A, while that in type B constituted 32 %. At a welding current of 280 A, these changed to 48 % for type A and 52 % for type B. For example, in the case of a welding current of 250 A with a large error, each droplet detachment period was seen to be not constant in Fig. 7a. At the beginning of the blue phase, the metal transfer mode was in type A, and each detachment period was longer. Subsequently, the mode changed to type B and the period became shorter from around 30 ms. Then, it changed again to type A after 50 ms. The results indicate that the occurrence of both the metal transfer modes significantly increases in the error.

3.2. Arc characteristics

To understand the effect of sodium content in the flux-cored wire on the arc characteristics, arc appearances were observed using a monochrome HSVC with bandpass filters for plasma line spectrums at welding currents of 190 A, 250 A and 310 A corresponding to the low, standard and high currents, and a color HSVC at 250 A.

As a general trend, the position of arc attachment reached the solid-liquid interface of the wire, thus covering part of the droplet during its formation at all the welding currents. The sodium has a lower boiling point of 1156 K and a lower ionization potential of 5.1 V, compared with 3134 K and 7.9 V for iron and 3558 K and 6.8 V for titanium, so the sodium vapor is more easily evaporated and able to strongly affect the arc characteristics, mainly by changing the electrical conductivity of the plasma. The result in Section 3.1 indicated that when the welding current was increased, the flux column length also increased. Accordingly, the molten metal couldn’t cover the flux column completely, thus making the area of the flux column surface exposed to the arc larger. The evaporation of sodium vapor is thereby enhanced, increasing the brightness and volume of the sodium plasma and affecting the metal transfer behavior. First, the effect of a mixture of sodium vapor and iron vapor in the plasma on arc characteristics is discussed for the standard current of 250 A based on the result of the above observations, and then those for 190 A and 310 A are considered to study the dependence on the current.

Figs. 8–11 show time-sequential images during 1 cycle of metal transfer observed using the HSVC equipped with Fe I, Ar I and Na I bandpass filters for wires 1 to 4 at 250 A. The welding current of 250 A was defined as a standard current, so the arc characteristics at this current are presented in detail with gas plasma (argon plasma) and metal vapor plasma (iron plasma and sodium plasmas). The metal transfer cycle period decreased from around 10 ms to 8 ms as sodium content increased from 0 % to 0.08 %, and then it increased again to 9.25 ms at 0.12 %. In the images for Na I in Fig. 8, weak arc radiation was still observed even though the sodium was not included in the flux. This is likely caused by the continuum spectrum or line spectra of other elements contained in the flux. It was already shown in [23] that the effect of the line spectrum of the gas plasma and iron plasma was negligibly small at this wavelength in the case of MCAW. Despite this background radiation, the sodium vapor behavior was clearly observed for wires 2–4 because of the intense radiation of the sodium plasma.

In the case of wire 1, the effect of iron plasma on the arc characteristics is relatively large because of the absence of sodium. The behavior of each metal plasma depended significantly on the type of

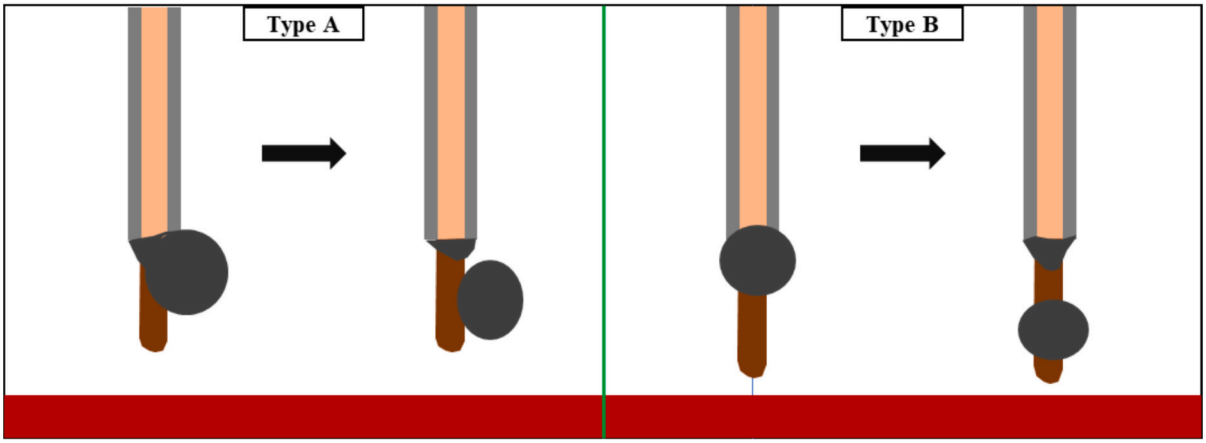

Fig. 6. Classification of two sub-modes in projected transfer mode [26].

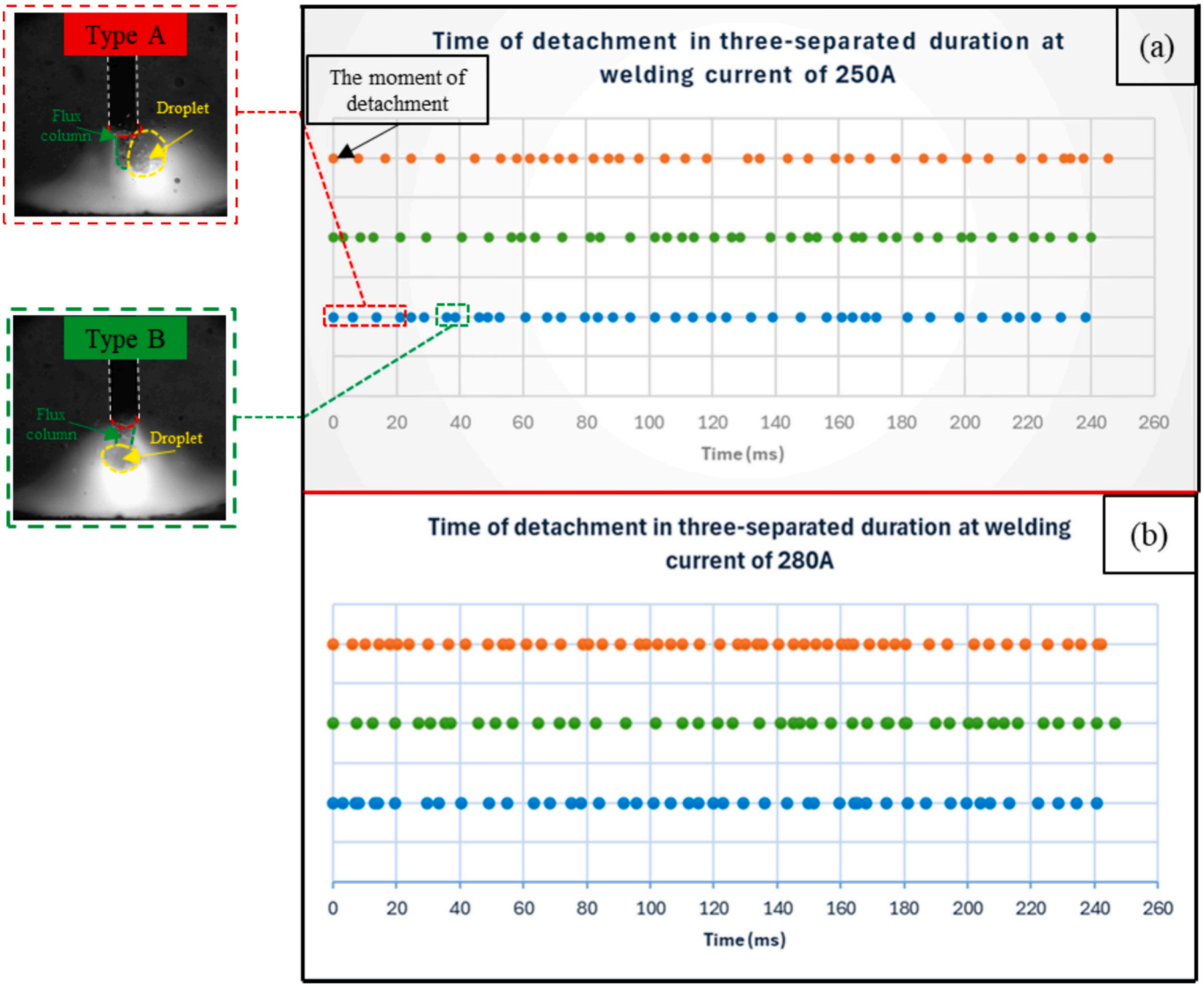

Fig. 7. Droplet detachment times in three separate periods for wire 3 at welding currents of (a) 250 A and (b) 280 A. (For interpretation of the references to color in this figure, the reader is referred to the web version of this article.)

metal. Iron mainly evaporated from the lower surface of the droplet and was widely distributed horizontally in the arc column. The amount of iron vapor produced changed according to the droplet growth process, decreasing around the time immediately before and after the droplet detachment (for example, 9 ms for wire 2, 8.25 ms for wire 3, and 8 ms for wire 4). This is thought to be because the temperatures of the detached droplets and the molten metal at the wire tip decreased as the droplets detached.

The sodium appears to evaporate mainly from both the flux surface and the droplet surface covering the flux. In the latter case, strong evaporation occurred stably from the pendant droplet at the wire tip. Since the flux at this position was covered by the droplet, the sodium in the flux could evaporate from the droplet surface via the inside of the droplet. In particular, in the case of high sodium content, sodium vapor tended to be concentrated in a narrow region around the flux near the central axis. When the lower part of the elongated flux was covered by large droplets over a wide area, the amount of sodium evaporated from this area decreased slightly (for example, 5.75 ms for wire 4).

The argon plasma had a much lower brightness than those of the iron and sodium plasmas, at least partly due to its lower number density (lower mole fraction) in the metal plasma. The argon plasma was seen to be distributed widely in the entire arc column and tended to overlap with the distribution of the iron plasma, as shown later in Fig. 12. This is similar to the characteristics of iron plasma distribution when droplets grow large in CO_2 arc welding using a solid wire [30].

A tendency presented in Figs. 8–11, but also seen in the overall measurement results, was that the type A mode was dominant in wires 1–3, which contained less sodium content, while the type B mode was typical in wire 4. There is a close relationship between the metal vapor behavior and the droplet formation and detachment processes. The important points can be summarized as follows: when droplets are formed on the side of the flux as in type A, the iron plasma distribution tends to be biased toward the droplet side, while the sodium plasma distribution tends to be biased toward the opposite flux side. When the droplets are formed at the center, as in type B, the sodium plasma is concentrated in a narrow region around the flux near the central axis. These observations strongly suggest that the difference in sodium plasma distribution has a strong effect on the current path in the arc.

Fig. 12 shows time-sequential color images of the arc appearances for wires from 1 to 4 during 1 cycle of metal transfer at 250 A. In the previous figures, the line spectrum distributions of each plasma were measured independently in different experiments, so it was difficult to compare them directly. Here, to clearly present the relative behavior of each plasma in a single image, observations using the color HSVC were

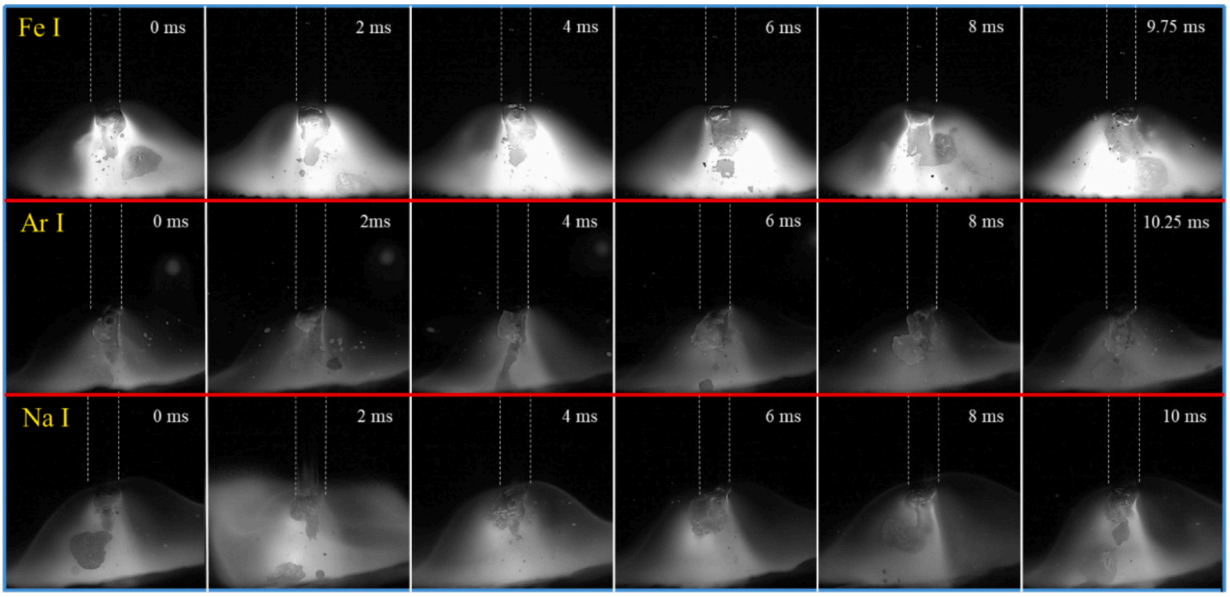

Fig. 8. Time-sequential images during 1 cycle of metal transfer observed using HSVC equipped with Fe I, Ar I and Na I bandpass filters for wire 1 at 250 A.

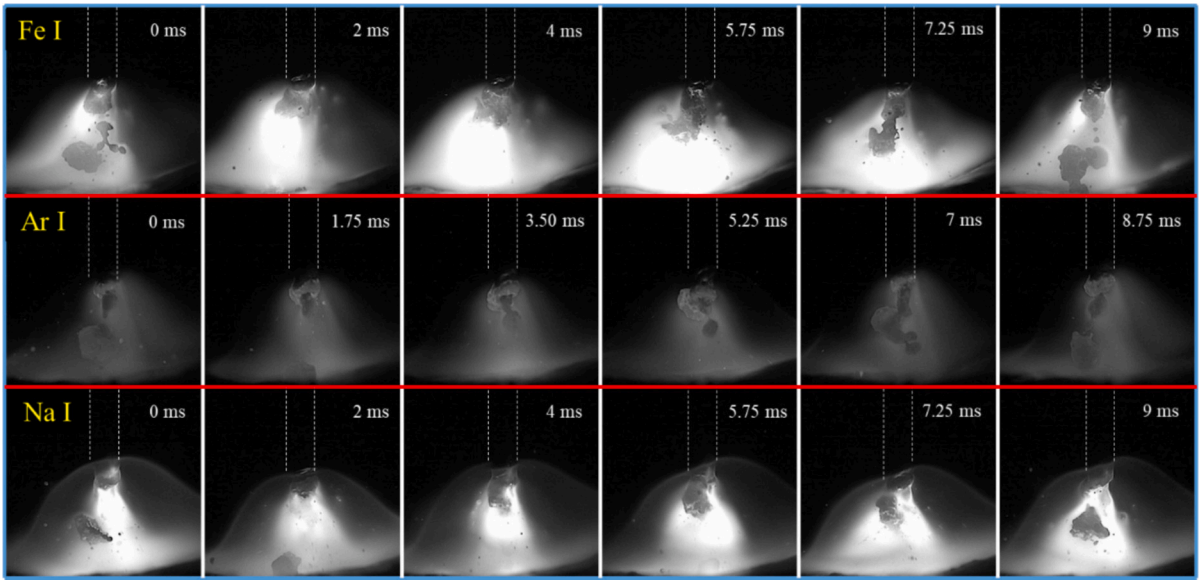

Fig. 9. Time-sequential images during 1 cycle of metal transfer observed using HSVC equipped with Fe I, Ar I and Na I bandpass filters for wire 2 at 250 A.

carried out.

In the figure, the radiation color of the shielding gas plasma should be red-purple because the shielding gas has a high proportion of argon. The radiation colors of iron plasma and sodium plasma are blue and brown (the latter corresponds to the wavelength of around 600 nm), respectively. A large part of the shielding gas plasma distribution was thought to overlap with the iron plasma distribution, making it difficult to distinguish each radiation source. The iron vapor evaporated mainly from the bottom of the droplet and was widely distributed throughout the arc, even though it became dense around the region under the droplet. The brown radiation emitted by sodium plasma was not observed in wire 1. As the sodium content increased, the brown radiation became more prominent, and the brightness of the arc decreased. The reason for the low brightness could be that the electrical conductivity of the arc increased due to the mixing of sodium vapor into the entire plasma, causing the arc temperature to decrease due to stronger radiative cooling. It was confirmed that the sodium evaporated strongly, especially in the period immediately before and after droplet detachment, in the vicinity of the droplet and flux. The observed behavior of the iron and sodium plasmas tended to agree with the results obtained using bandpass filters.

Fig. 13 shows a detailed comparison of the typical arc appearances for wire 1, wire 3 and wire 4 at 250 A, including the flux column, molten metal and droplet. The sodium content of 0.08 % was used because the maximum metal transfer frequency was achieved with this content. The contours showing iron plasma and sodium plasma represent areas of particularly high brightness. In the cases of wires 1 and 3, the characteristics were similar to those in the type A mode, in which droplets were formed on the side of the flux. It can be seen that the iron plasma was widely distributed on the droplet side, while the sodium plasma was concentrated near the flux on the opposite side. In the case of wire 4, the characteristics were those of the type B mode, where the droplet was formed near the center to cover the flux. The sodium plasma was concentrated around the flux and distributed from the bottom of the

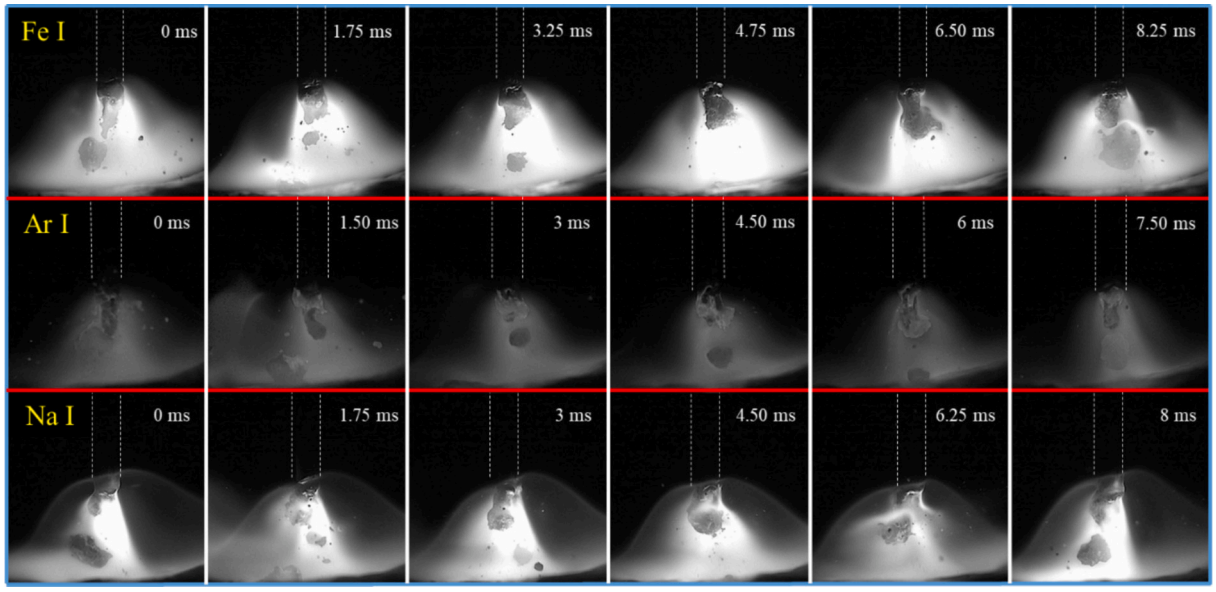

Fig. 10. Time-sequential images during 1 cycle of metal transfer observed using HSVC equipped with Fe I, Ar I and Na I bandpass filters for wire 3 at 250 A.

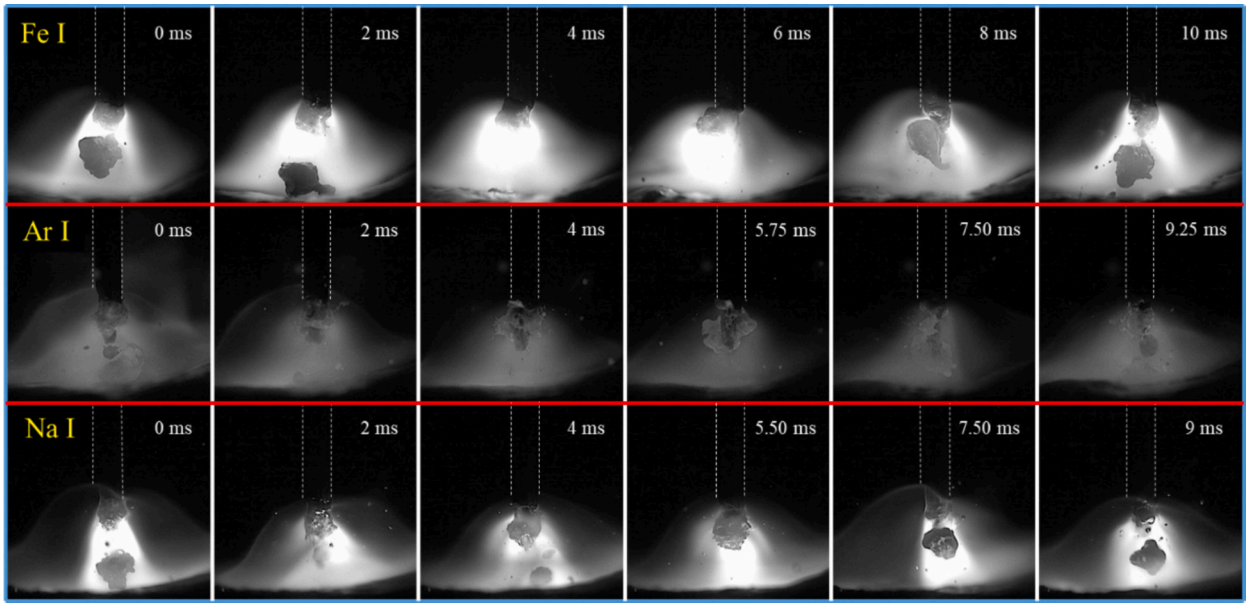

Fig. 11. Time-sequential images during 1 cycle of metal transfer observed using HSVC equipped with Fe I, Ar I and Na I bandpass filters for wire 4 at 250 A.

droplet to the weld pool. The iron plasma was widely distributed in the arc column.

The arc appearance at the standard current of 250 A was presented in detail. Following this, the influence of the current is also discussed, focusing on 190 A and 310 A.

Fig. 14 shows the time-sequential images during 1 cycle of metal transfer observed using HSVC equipped with the Na I bandpass filter for wires from 1 to 4 at 190 A. Fig. 15 shows a detailed comparison of the typical arc appearances for wire 1, wire 3 and wire 4 at 190 A, also representing regions of the flux column, molten metal and droplet. In this case, the periods of metal transfer were stable: 16.50 ms, 15.75 ms, 15.00 ms and 16.00 ms for sodium contents of 0 %, 0.04 %, 0.08 % and 0.12 %, respectively. As sodium content increased from 0.04 % to 0.12 %, the spectral intensity of sodium plasma near the central axis gradually increased. The metal transfer mode was almost in type A for all wires. For all wires, when droplets were formed on the side of the flux, iron vapor evaporated from the bottom of the droplet and was distributed with a bias toward the droplet side, while sodium vapor evaporated in large amounts from the flux and was distributed mainly on the opposite side from the iron vapor. Thus, it was found that the distributions of iron plasma and sodium plasma were clearly separated. When the wire contained sodium, the flux column became longer, and the spectral intensity of sodium tended to become larger in the period before and after droplet detachment under all conditions.

Fig. 16 shows the time-sequential images during 1 cycle of metal transfer observed using HSVC equipped with the Na I bandpass filter for wires from 1 to 4 at 310 A. Fig. 17 shows the detailed comparison of the typical arc appearances for wire 1 and wire 4 at 310 A, also representing regions of the flux column, molten metal and droplet. In this case, the periods of metal transfer were very short: 3.75 ms, 4.75 ms, 5 ms and 5.50 ms for sodium contents of 0 %, 0.04 %, 0.08 % and 0.12 %, respectively. The brightness of the sodium plasma became stronger with

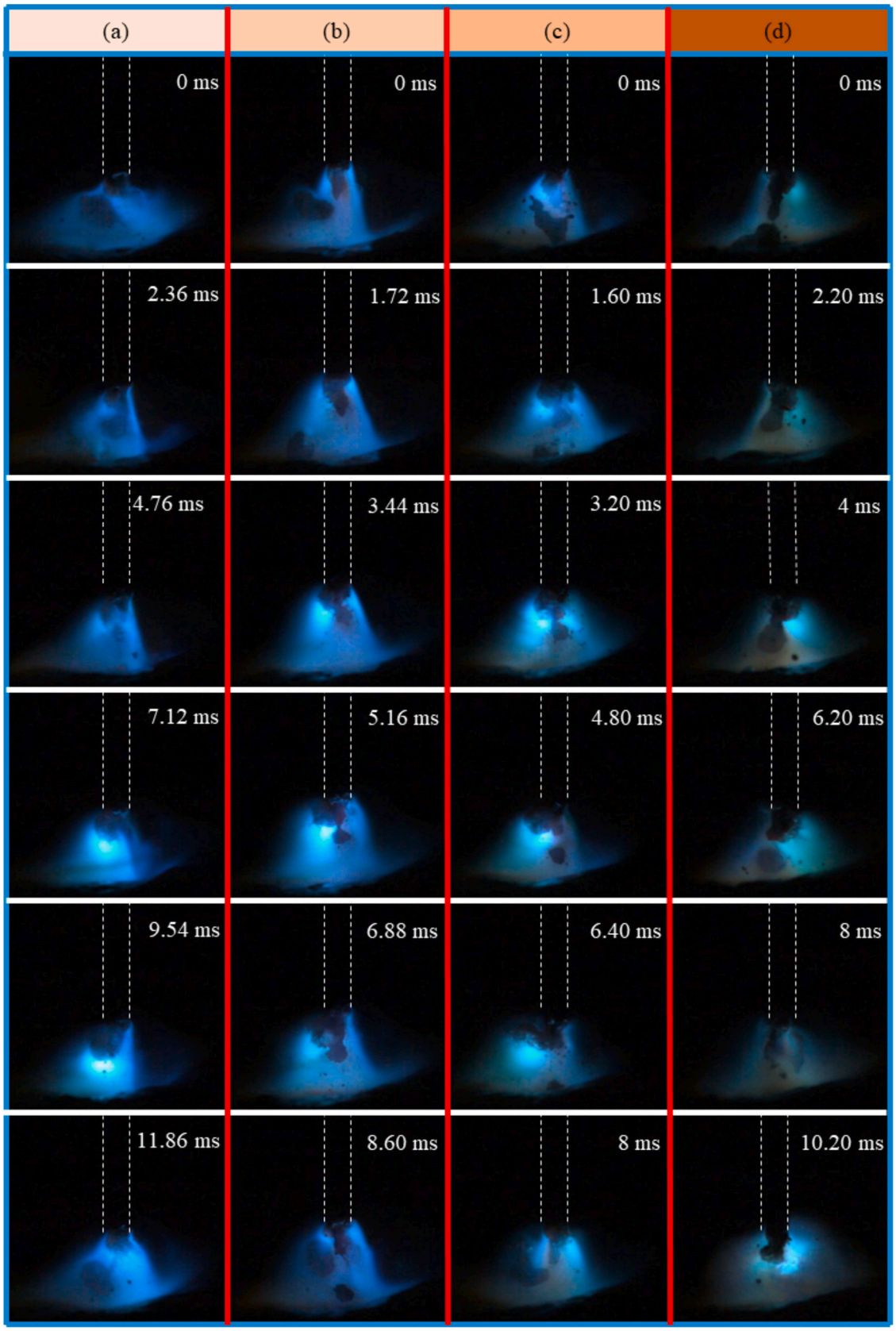

Fig. 12. Time-sequential color images of arc appearances for wires from 1 to 4 during 1 cycle of metal transfer at 250 A. (For interpretation of the references to color in this figure, the reader is referred to the web version of this article.)

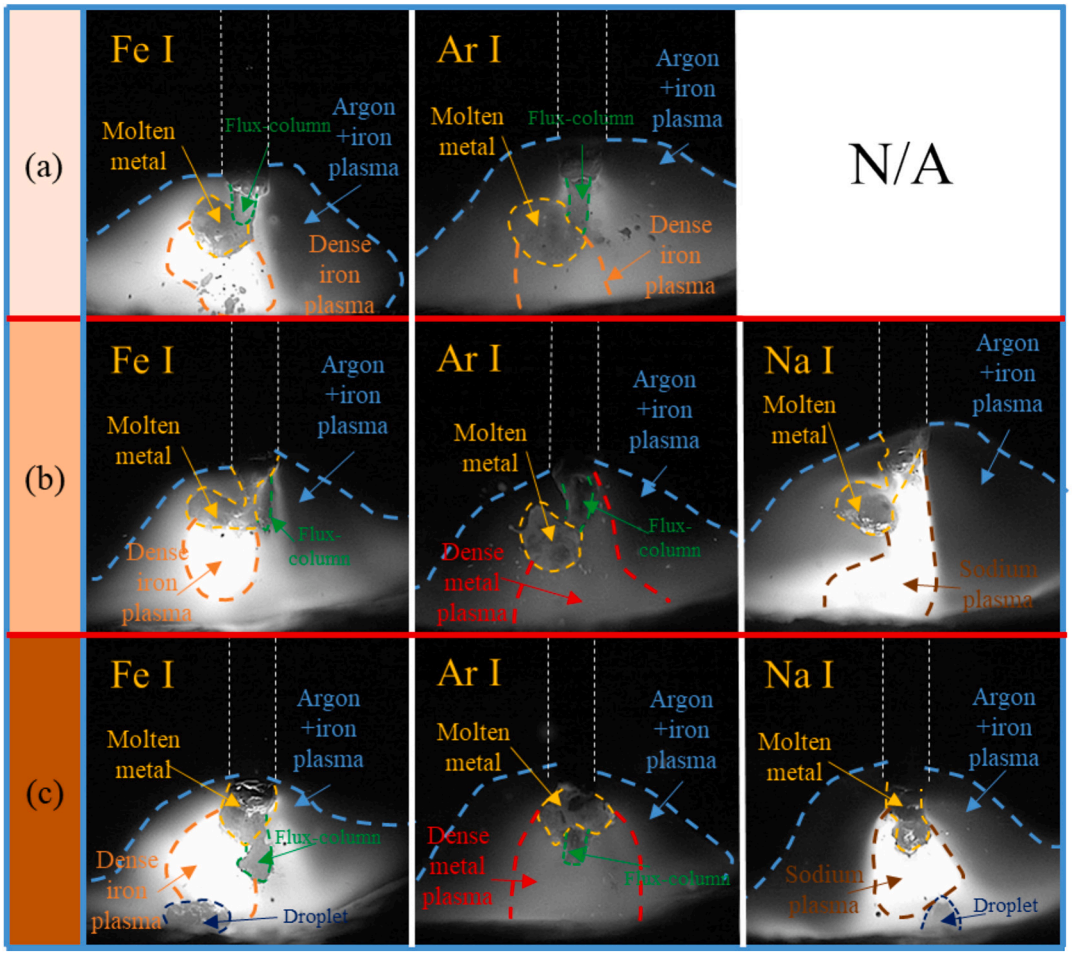

Fig. 13. Detailed comparison of the typical arc appearances for (a) wire 1, (b) wire 3 and (c) wire 4 at 250 A, including the flux column and molten metal.

an increase in sodium content and was also stronger than for lower currents. The iron plasma covered the upper part of the droplet, while the sodium plasma was constricted to the center under the droplet, and the degree of constriction increased with sodium content. The droplet was mainly formed at the central region and then moved gradually downward along the flux column, in accordance with the type B sub-mode, in all wires. The intensive heat input to the wire due to the high current enhanced the melting rate of the iron sheath, while the melting rate of the flux by thermal conduction from the surrounding molten metal will not be significantly changed. Therefore, the difference between the melting rates of the metal and flux is increased, leading to the longer flux column at the higher current. The exposed long flux column was heated and melted mainly by thermal conduction from the arc. This point will be discussed in detail in the next section. The flux tended to detach right after or together with the droplet.

3.3. *The effect of sodium vapor on the metal transfer behavior*

In this section, the effect of sodium vapor on metal transfer behavior is discussed based on the experimental results presented in the previous sections. The processes of droplet formation and detachment in FCAW are governed by the heat and force balances between the wire and the arc. The evaporation of sodium vapor is related to both balances but has a particularly decisive effect on the force balance.

First, the heat balance is considered. The main factors that cause the temperature increase of the wire are Joule heating in the wire, thermal conduction from the high-temperature arc, and electron condensation heating as current flows from the wire to the arc. Since the electrical conductivity of the sheath metal is much greater than that of the flux, the Joule heating and electron condensation heating mainly occur in the sheath metal, where most of the current flows. The main factors leading to the decrease in temperature of the wire are heat losses due to the evaporation of the molten metal and flux, and droplet detachment. When the flux contains a low boiling point element such as sodium, the effect of heat loss due to evaporation is particularly large. In addition, the sodium vapor that evaporates and mixes with the arc causes changes in the temperature field and current path in the arc, as described below.

In this way, most of the heat input to the wire is transferred to the sheath metal, which melts first, forming metal droplets. On the other hand, the heat input to the flux is smaller, so the melting rate is slower than that of the sheath, which leads to the formation of a flux column. The main reason that the flux column becomes longer as the current increases is likely to be because the electron condensation heats the metal sheath and is proportional to the current. The flux inside the sheath is heated by thermal conduction, which is relatively weak, so it is protected by the sheath. Arc heating will be similar for the metal sheath and the exposed flux column.

Next, the force balance is considered. In GMAW using a solid wire, the main forces acting on the metal droplet are the surface tension, arc pressure, plasma shear force, gravity and Lorentz force [31]. The surface tension and arc pressure are upward forces that hold the droplet in place and are of roughly equal magnitude. The arc pressure is formed by the Lorentz force acting within the arc, which increases as the current path becomes concentrated directly below the droplet. The plasma shear force is a downward force generated by friction between the droplet and the plasma flow around it. This force is an order of magnitude smaller

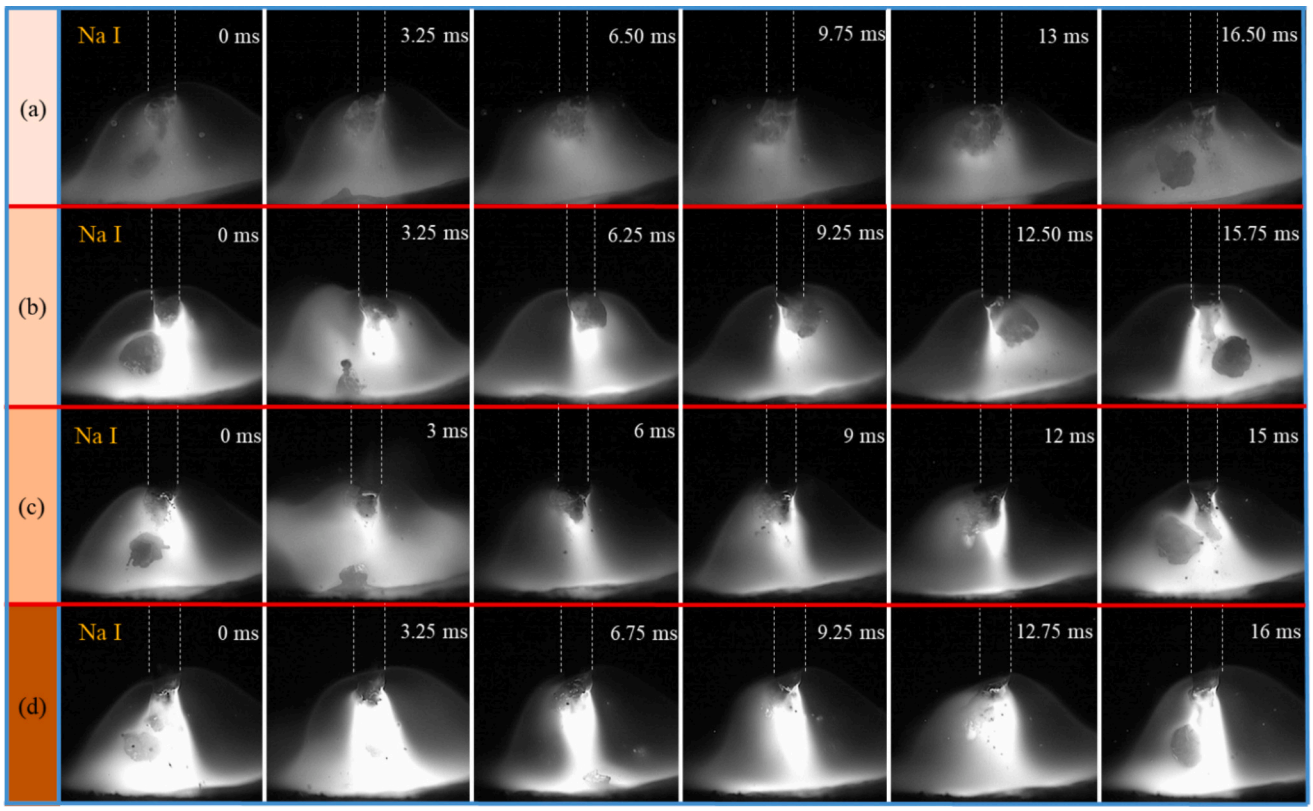

Fig. 14. Time-sequential images during 1 cycle of metal transfer observed using HSVC equipped with the Na I bandpass filter for (a) wire 1, (b) wire 2, (c) wire 3 and (d) wire 4 at 190 A.

than the surface tension and arc pressure and is generally considered negligible. The gravity is also a downward force, which is especially effective in low current. The magnitude and direction of the Lorentz force acting on a droplet depend on the current path in the droplet. If the current path in the droplet expands downward in a cone shape, the force is downward and inward, but if it has only a vertical component, the force is inward. The current path in the droplet is determined by the electrical conductivity field of the arc surrounding the droplet.

In FCAW, when the flux contains elements such as sodium with low boiling point and low ionization energy, the current path has a strong effect on the force balance, particularly through the following two mechanisms. The first is the strong upward recoil pressure associated with the intensive downward evaporation of sodium vapor. In laser keyhole welding, the laser focal point on the surface of the weld pool is strongly heated, so the metal vaporizes rapidly due to the localized heating reaching near the boiling point. The resulting recoil pressure pushes down the surface of the weld pool, forming a keyhole [32]. In FCAW, the droplet is pushed upward by a similar effect. The magnitude of this recoil pressure will be estimated with a simple model later.

The second point is the change in the electrical conductivity of the plasma that occurs when the sodium vapor is mixed into the plasma. Fig. 18 shows the dependence of electrical conductivity of sodium, iron and shielding gas plasmas on temperature. The data for the shielding gas mixture is obtained using the methods presented in [33,34], and that for iron in [35]. Similar methods were used for the Na data: the phenomenological potential [36] was used to describe the Na—Na and elastic $Na\text{-}Na^{+}$ interactions, with the polarizability of Na taken from [37]; charge transfer cross-sections [38] were used for the inelastic $Na\text{-}Na^{+}$ interaction, and momentum-transfer cross-sections [39] were used for the e-Na interaction. It is well known that the mixing of a small amount of iron vapor into a shielding gas plasma such as argon significantly increases its electrical conductivity at low temperatures [40]. In the case of sodium vapor, because the ionization energy of the sodium atom is much smaller than that of the iron atom, the increase in electrical conductivity due to the mixing becomes even greater. The boiling point of titanium and the ionization energy of its atom, which are the main component of the flux, are closer to those of iron than to those of sodium. Therefore, it is implicitly assumed that the characteristics of a titanium plasma are closer to those of iron plasma in the following discussion. In the case of GMAW using a solid wire, a significant temperature drop occurs due to the strong radiation loss in the plasma containing dense metal vapor near the arc axis. This causes a decrease in the electrical conductivity of the plasma. Accordingly, part of the current conducts in the surrounding shielding gas plasma, avoiding the iron plasma. In contrast, in metal plasmas containing high concentrations of sodium vapor, the electrical conductivity increases further, making it easier for the current to flow through the metal plasma. As a result, it is expected that the current path tends to concentrate near the central axis, so the Lorentz force inside the droplet acts inward. The increase in current density at the bottom of the droplet leads to an increase in arc pressure.

Fig. 19 shows a schematic of the relationship between the arc appearance, current path, and droplet formation at welding currents of 190 A, 250 A, and 310 A for wire 4 to illustrate the effect of current. Wire 4 is used because it is most susceptible to the effects of sodium vapor. As mentioned above, the metal transfer was almost fully in type A sub-mode at 190 A. When the current is small, the Lorentz force acting on the droplet is small, and the effect of surface tension is relatively large, so the molten sheath metal forms a droplet on the side of the flux. The Lorentz force becomes larger at 250 A, so the droplet is pushed downward toward the central axis, and the proportion of metal transfer in type B sub-mode gradually increases. When the current rises, the arc pressure pushing up the droplet increases, and the recoil pressure also increases with the sodium vapor formation. The Lorentz force becomes even stronger at 310 A, so the droplet is always formed on the central axis, leading to stable metal transfer in type B sub-mode. As the heat input to the wire increases, sodium vaporization increases significantly,

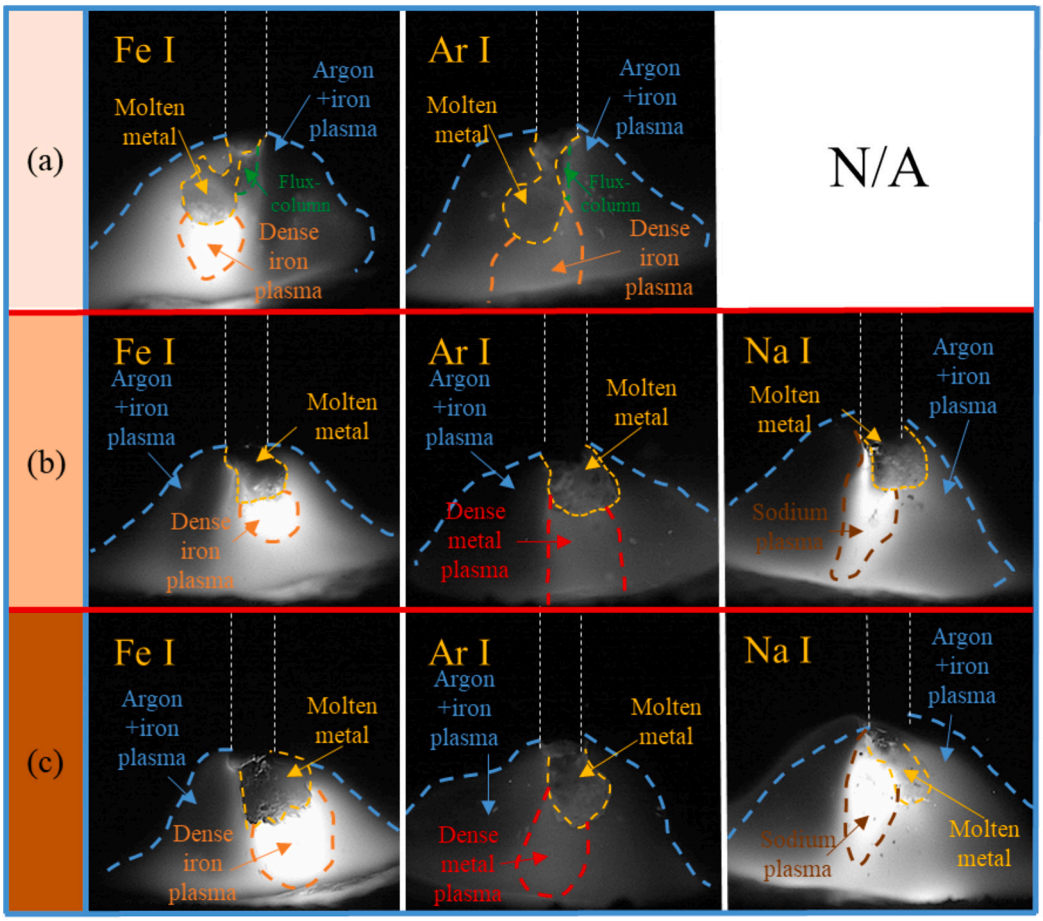

Fig. 15. A detailed comparison of the typical arc appearances for (a) wire 1, (b) wire 3 and (c) wire 4 at 190 A, including the flux column and molten metal.

and a metal plasma containing a high concentration of sodium vapor is formed on the central axis. This constricts the current path in the arc into the central axis, enhancing the recoil pressure caused by the sodium vaporization and the arc pressure.

Fig. 20 shows a schematic of the relationship between the arc appearance, current path and droplet formation for wire 1, wire 2 and wire 4 at a welding current of 250 A to illustrate the effect of sodium content in the wire. The standard current of 250 A is chosen for the comparison. The type A and type B sub-modes were mixed at 250 A, and the proportion of metal transfer in type B sub-mode increased, especially for wire 4. This is related to the increase in sodium vaporization with the sodium content. The mixing of sodium vapor increases the electrical conductivity of the metal plasma near the central axis, causing the current path to concentrate in this region. Accordingly, the mixing increases the inward Lorentz force, causing the metal transfer to approach the type B sub-mode.

The reason for the maximum of the metal transfer frequency occurring for wire 3, as presented in Fig. 4, is also discussed. When sodium content was smaller or larger than the content corresponding to the maximum transfer frequency, the type A and B sub-modes became dominant, respectively. The content corresponding to the maximum decreased when the current increased, as shown in Fig. 21. For wire 2, sodium evaporates mainly from the side of the flux column opposite the droplet and is transported into the arc, greatly increasing the electrical conductivity of the plasma around the flux column. As a result, part of the current flows from the wire through the sodium plasma to the weld pool, so the current flowing from the bottom of the droplet to the arc decreases, leading to the lower arc pressure under the droplet. In this case, since the amount of sodium vaporized from the droplets is small, the effect of the recoil pressure acting on the droplet is relatively small. Consequently, the metal transfer frequency tends to increase compared to that of wire 1. On the other hand, when the sodium vapor production increases significantly, as in the case of wire 4, the recoil pressure acting on the droplet increases, and the current density at the bottom of the droplet increases due to the concentration of current in the arc, causing the arc pressure to rise. Therefore, the metal transfer frequency tends to decrease. Due to the balance of these factors, the metal transfer frequency has a maximum at wire 3.

The above discussion makes clear that the vaporization of sodium has a strong effect on the metal transfer behavior. Here, the effect of sodium vaporization on the current waveform, which is one of the important indicators of arc stability, is discussed.

Fig. 22 shows the waveforms of welding voltage, welding current and the sodium intensity (maximum and mean values) for wires 1 and 4, corresponding to sodium contents for the maximum and minimum metal transfer frequencies at the welding current of 310 A. The sodium intensity is identified based on the brightness of the image in the movie using the ImageJ software. For convenient discussion, the welding voltage and mean Na I intensity, which was calculated as the integrated intensity over the image divided by the total pixels, are graphed on the primary axis. The welding current and maximum Na I intensity are shown on the secondary axis.

Since the welding power source was operated with constant voltage, the arc voltage for both wires was almost constant. The current waveform for wire 1, which does not contain sodium in the flux, has a smaller amplitude of fluctuation than that for wire 4, with the largest sodium content. The intensity of Na I for wire 1 was caused by the background radiation, as mentioned in the previous section. The maximum intensity and the mean intensity for wire 1 were about 100 and 70 on average, respectively, while those for wire 4 were about 200 and 130 on average,

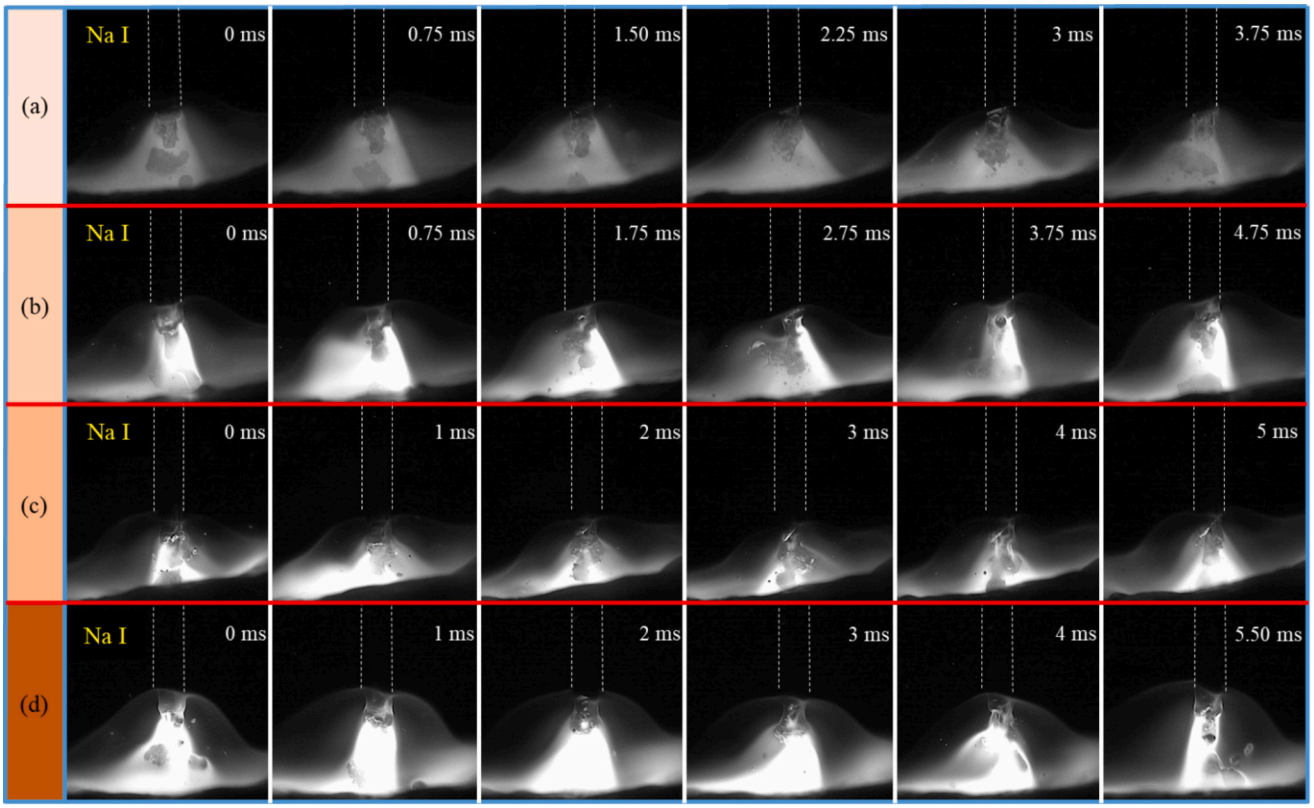

Fig. 16. The time-sequential images during 1 cycle of metal transfer observed using HSVC equipped with the Na I bandpass filter for wires from 1 to 4 at 310 A.

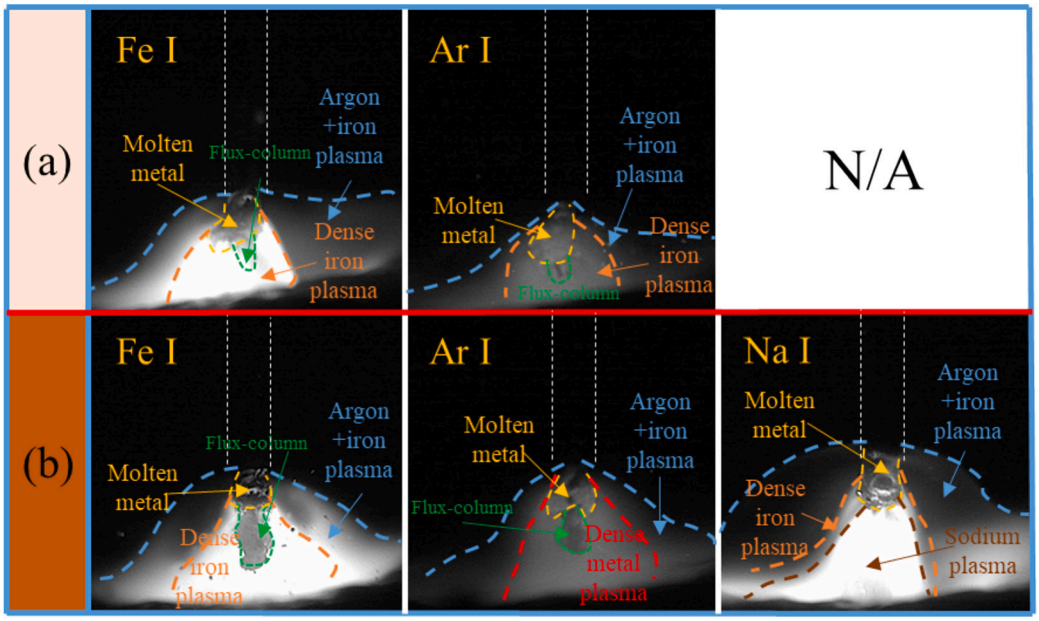

Fig. 17. A detailed comparison of the typical arc appearances for (a) wire 1 and (b) wire 4 at 310 A, also representing regions of the flux column, molten metal and plasmas.

respectively. Therefore, the actual intensities after subtracting the background were about 100 and 60, respectively, indicating the presence of a significant sodium vapor concentration. The amplitude of the current fluctuation was also larger for wire 4. Under the constant voltage conditions, the current fluctuation indicates a change in the current path or arc length. Therefore, an increase in sodium content at 310 A not only decreased the metal transfer frequency but also impaired the arc stability.

Fig. 23 shows schematic illustrations of the typical behavior of the current waveform fluctuation and metal transfer in MCAW and FCAW, allowing the current fluctuation mechanisms to be compared. This figure also shows the relationship between the arc attachment positions and current paths at the moments of maximum and minimum currents. The case of wire 1 without sodium vapor is considered for simplicity.

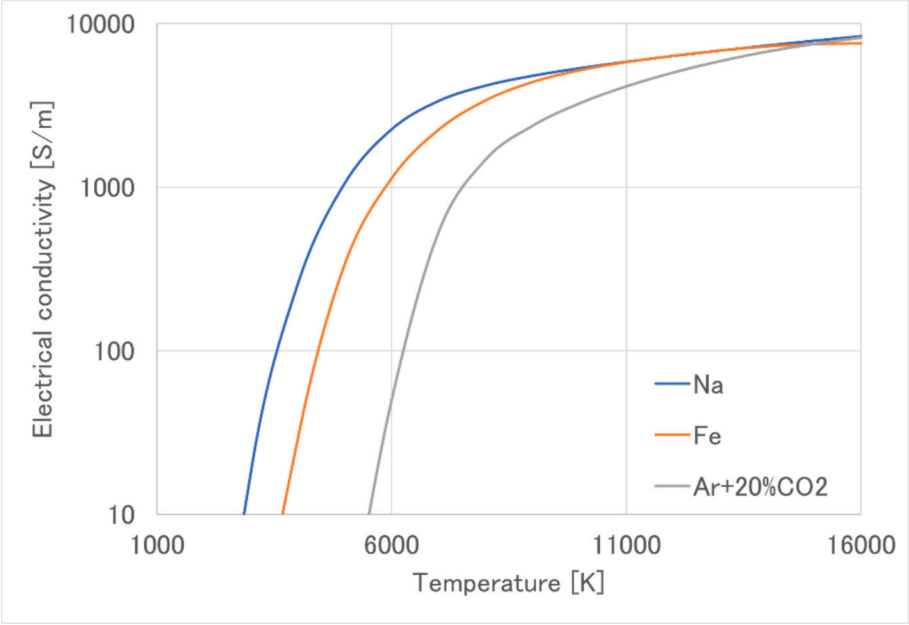

Fig. 18. Dependence of electrical conductivity of sodium, iron and shielding gas plasmas on temperature.

The fluctuation of the current waveform in FCAW is generally smaller than that in MCAW in the free flight transfer mode [23], reflecting the smaller change in the arc length. In MCAW, the melting rate of the metal flux is higher than that of FCAW, so the tip of the flux column is located slightly lower than the tip of the sheath and is often covered with a droplet [20]. Therefore, the droplet tends to form axisymmetrically around the central axis, as in GMAW with a solid wire. As the droplet grows, it is elongated downward by the Lorentz force and forms a neck. When the current density at the neck increases, the Lorentz force prompts the droplet detachment, and the arc attachment at the bottom of the droplet moves back to the wire tip after the detachment. Because the arc length changes significantly due to this droplet behavior, the amplitude of the current fluctuation increases accordingly. In contrast, a flux column extends toward the weld pool on the central axis in FCAW, and droplets are formed on the sides or around the flux column. Since the flux column has low electrical conductivity, the cross-sectional area of the current flowing from the sheath through the neck to the droplet becomes smaller, resulting in an increase in the current density. As a result, the droplet is more easily detached, the change in arc length is smaller, and the amplitude of the current fluctuation is also reduced. According to a previous study [23], the metal transfer frequency in MCAW at 220 A is 27.6 Hz, which is about 37 % of the 75.1 Hz measured in the current work. For the above reasons, FCAW is considered to have better stability than MCAW.

Next, the recoil pressure generated by sodium vaporization is roughly estimated and compared with other driving forces acting on the droplet. The vapor is assumed to contain only Na for simplicity, even though the actual composition is thought to be a mixture of Na, Na_2O, and other minor components. The magnitude of the recoil pressure corresponds to the momentum of the vapor which is calculated by dividing the product of the mass of vapor per unit time (m_{Na_tot}) [kg/s] and the evaporation velocity, assumed to be the thermal velocity (v_{na}) [m/s], by the area over which the pressure is applied (S_{Na}) [m^2]. Each is calculated using the following formula:

$$m_{Na\_tot} = v_{wf} m_{wire} F_{Na} \tag{1}$$

$$v_{Na} = \sqrt{\frac{8kT}{\pi m_{Na}}} \tag{2}$$

$$s_{Na} = \pi r_{wire}{}^2 \tag{3}$$

where v_{wf} is the wire feeding speed [m/s], m_{wire} is the mass of wire per unit length [kg/m], F_{Na} is the mass fraction of sodium atom in wire, k is the Boltzmann constant [J/K], T is the temperature of sodium vapor [K], m_{Na} is the mass of a sodium particle [kg], and r_{wire} is the wire radius [m]. Two sodium vapor temperatures were considered; the boiling point of sodium and the maximum temperature of the droplet, which was assumed to be the same as that measured in GMAW using an Ar-CO_2 shielding gas mixture (around 2600 K) [41]. In principle, S_{Na} represents the surface area of the arc attachment, but here it is assumed to be equal to the wire cross-sectional area for simplicity.

The standard current of 250 A is used for the purposes of discussion. It is assumed that all the sodium in the wire evaporates from the droplet surface.

Fig. 24 shows the minimum and maximum recoil pressures acting on the droplet as a function of the sodium content. The recoil pressure increases with increasing sodium content and droplet temperature, varying between approximately 500 Pa and 2400 Pa. In the case of GMAW using a solid wire and Ar-20%CO_2 mixture shielding gas, the arc becomes more constricted than that in pure argon shielding gas due to the higher specific heat. As a result, the arc pressure becomes higher (around 1000 Pa in Ar-20%CO_2 compared to 500 Pa in argon) [42]. As mentioned above, in the case of GMAW using a solid wire, the driving forces regarding the droplet behavior are dominated by the surface tension and arc pressure and Lorentz force, those might be of the same order of magnitude. The recoil pressure is smaller than the arc pressure for wire 2, but both are roughly the same for wire 3, and the recoil pressure is expected to be greater for wire 4. As a result, it was shown that when a large amount of sodium element is added to the flux within the range of sodium content of the prototype wires, the recoil pressure due to sodium vaporization has a large effect on the metal transfer behavior.

The findings of this study proved that the addition of a small amount of sodium to the flux can enhance the metal transfer frequency in FCAW, improving the welding stability. However, the welding process might become unstable if the added amount is excessive, mainly due to the increased recoil pressure acting on the bottom of the droplet, which results from the intensive sodium vaporization. This relationship strongly depends on welding parameters like the welding current, so

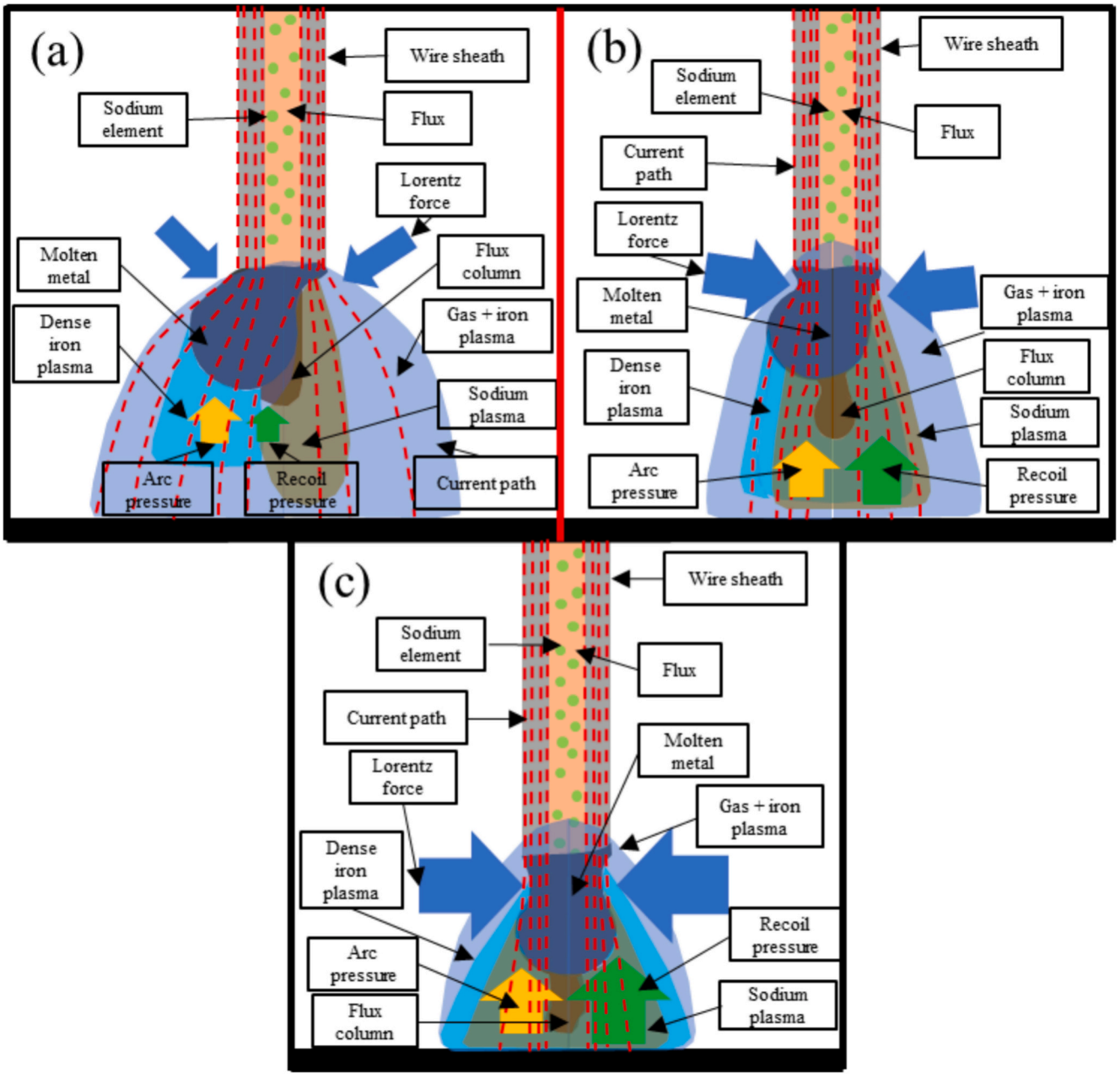

Fig. 19. Schematic of relationship between arc appearance, current path and droplet formation at welding currents of (a) 190 A, (b) 250 A and (c) 310 A for wire 4.

optimizing the sodium content in the flux is found to be decisively important for stabilizing the welding process.

4. Conclusion

In this study, four types of prototype flux-cored wires with different sodium contents in the flux were fabricated. By using these wires, the influence mechanism of sodium element on the metal transfer behavior was elucidated through the shadowgraph measurement of the metal transfer behavior as well as spectroscopic and color image observation of the arc characteristics. The main conclusions can be summarized as follows:

1. The metal transfer between 190 A and 310 A was in the projected transfer mode and further classified into two sub-modes (type A and type B) based on the droplet formation process. A larger droplet was formed on the side of the flux column in type A, while a smaller one was formed in the center, covering the flux in type B. The metal transfer frequency became larger in the latter case for the same wire feeding speed.
2. Type A tended to dominate under the lower current and lower sodium content conditions, while type B dominated under the opposite conditions. The dominant sub-mode was determined depending on the Lorentz force acting on the droplet. At the medium current (250 A and 280 A), both sub-modes appeared in similar proportions.
3. The metal transfer frequency is maximum at a particular sodium content. When the sodium content was smaller or larger, type A and type B sub-modes became dominant, respectively. The content corresponding to the maximum frequency decreased with increasing current.
4. In type A sub-mode, the iron plasma was widely distributed on the droplet side of the flux, while the sodium plasma was concentrated near the flux on the opposite side, so both were separated. On the contrary, in type B, the sodium plasma was concentrated around the

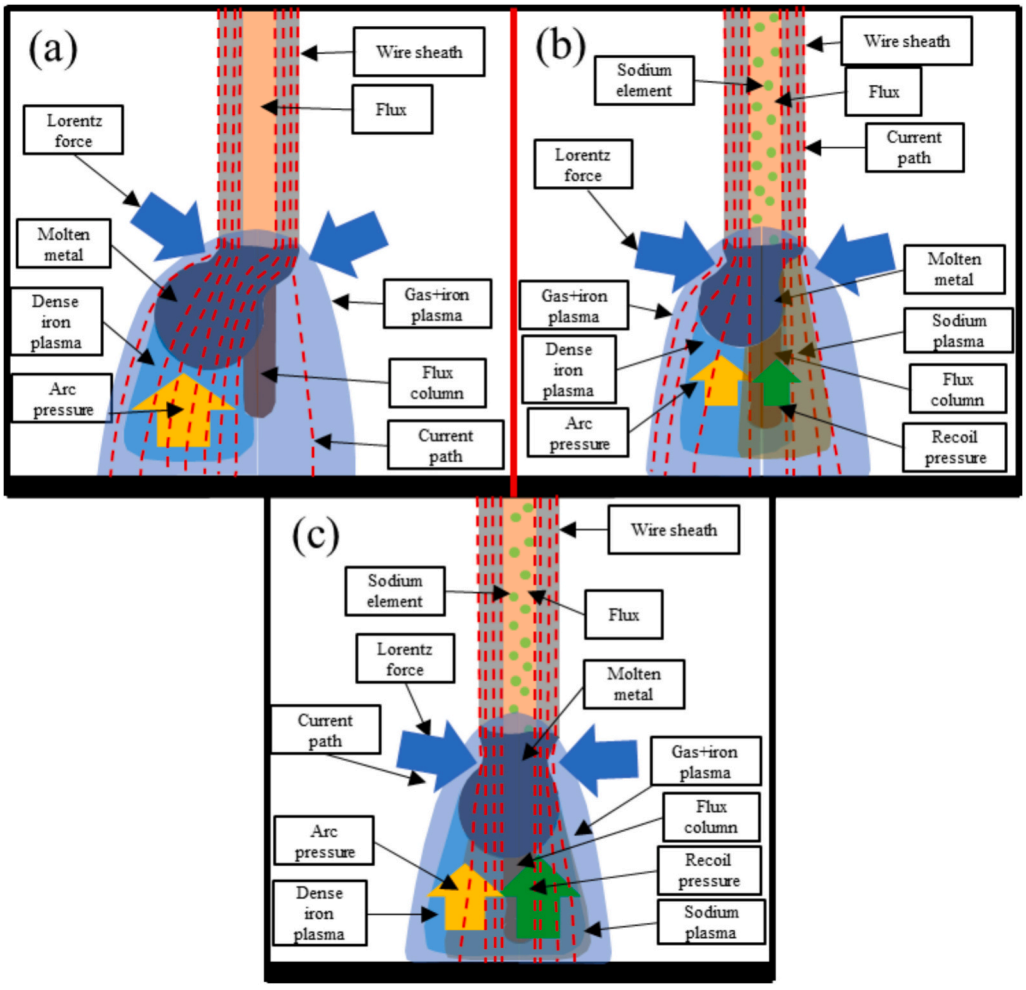

Fig. 20. Schematic of relationship between arc appearance, current path and droplet formation for (a) wire 1, (b) wire 2 and (c) wire 4 at welding current of 250 A.

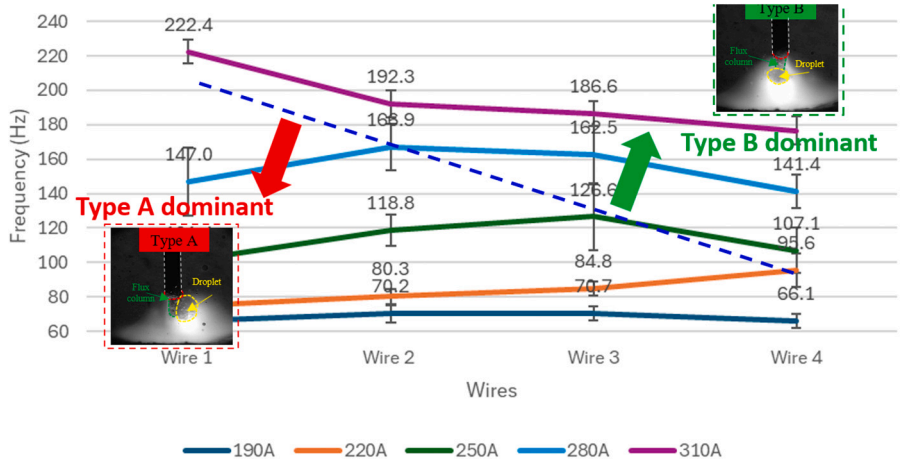

Fig. 21. A schematic showing the dominant sub-modes.

flux at the center, and the iron plasma was widely distributed in the arc column, so both overlapped around the center.

5. The sodium has a low boiling point and low ionization potential. In type A sub-mode, the sodium vapor significantly increased the electrical conductivity of plasma around the flux column, so part of the current flowed from the wire through the sodium plasma to the weld pool. Accordingly, the current flowing through the bottom of the droplet to the arc decreased, leading to the lower arc pressure and recoil pressure under the droplet and increasing the metal transfer frequency with sodium content. On the other hand, in type B, the sodium vaporization increased around the center, increasing the recoil pressure. In addition, the current density at the bottom of the droplet increased due to the current concentration in the arc, causing the arc pressure to rise. Therefore, the metal transfer

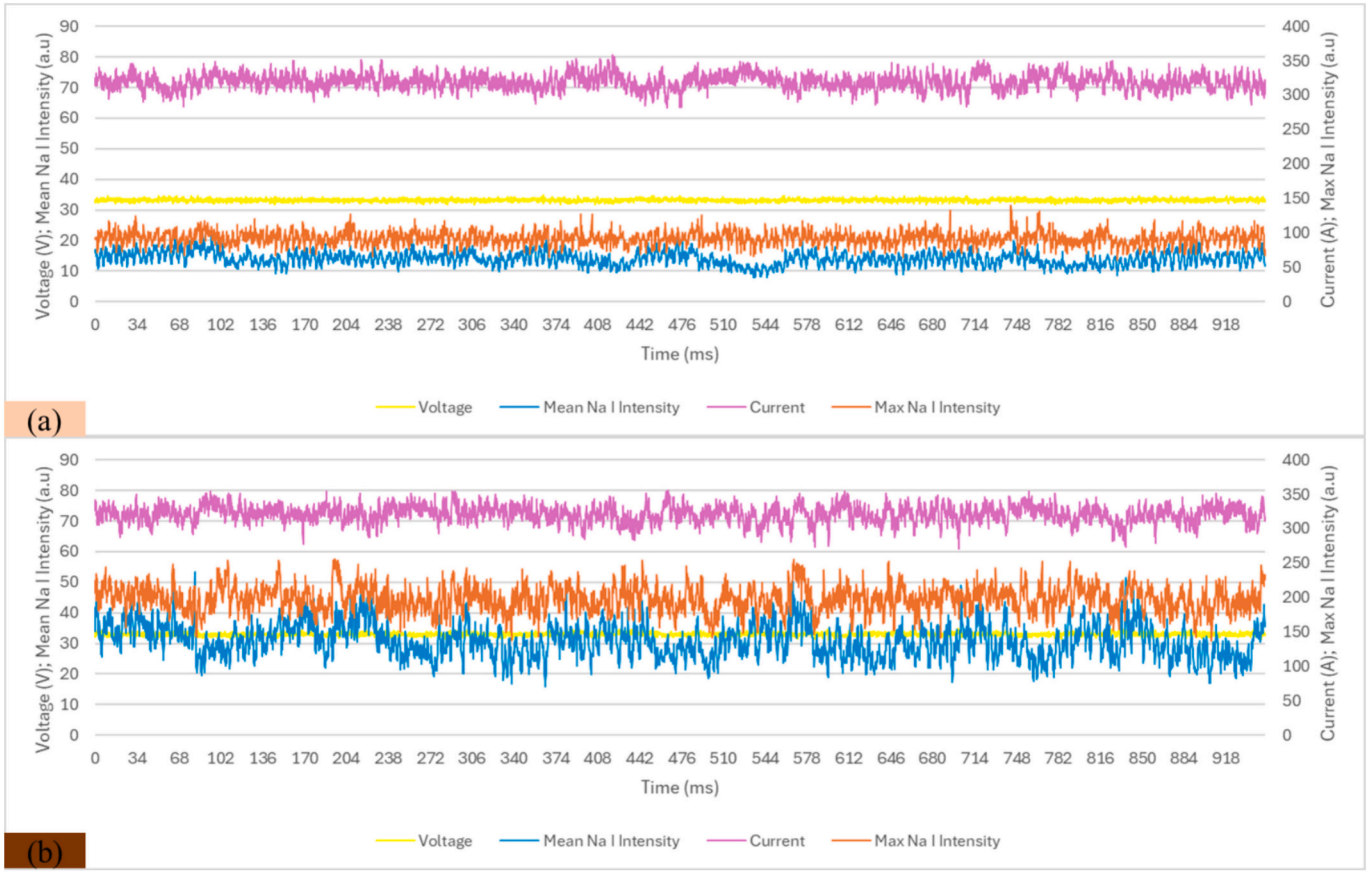

Fig. 22. Current, voltage and intensity waveform for (a) wire 1 and (b) wire 4 at welding current of 310 A.

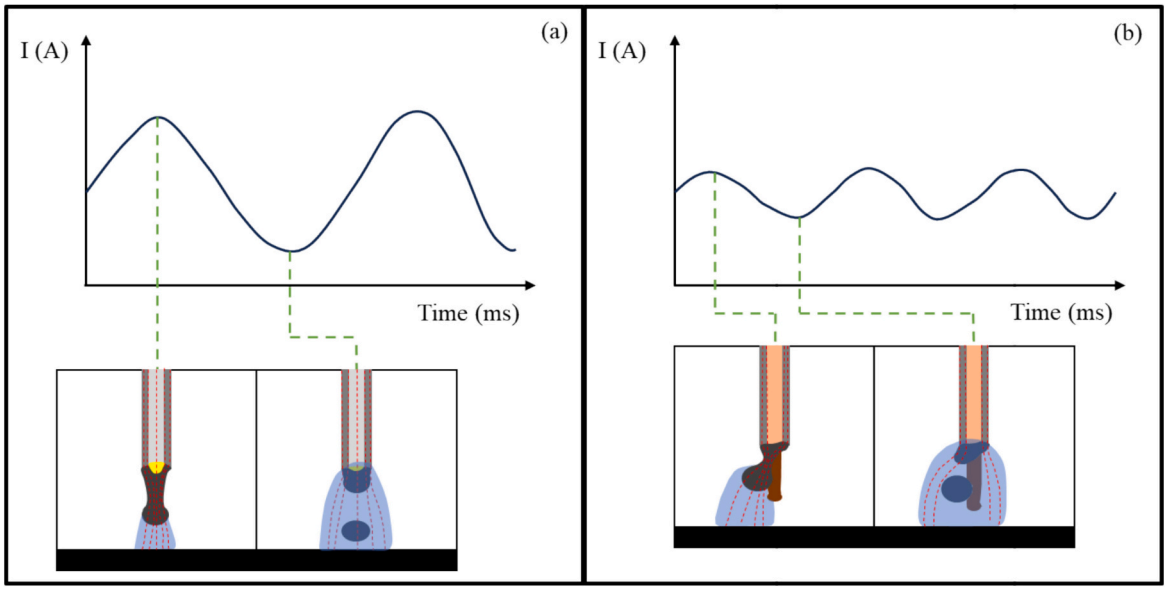

Fig. 23. Schematic illustrations of the typical behaviors of the current waveform fluctuation and metal transfer in (a) MCAW and (b) FCAW.

frequency tended to decrease with sodium content. Due to the balance of these factors, the metal transfer frequency became a maximum at a particular sodium content.

Adding a small amount of sodium to the flux can increase the metal transfer frequency in FCAW and improve the welding stability. However, too much sodium can increase the recoil pressure acting on the bottom of the droplet, which may decrease stability. The results and analysis presented will assist in selecting the optimum sodium content to stabilize the welding process.

CRediT authorship contribution statement

Dang Khoi Le: Writing – original draft, Investigation. **Shinichi**

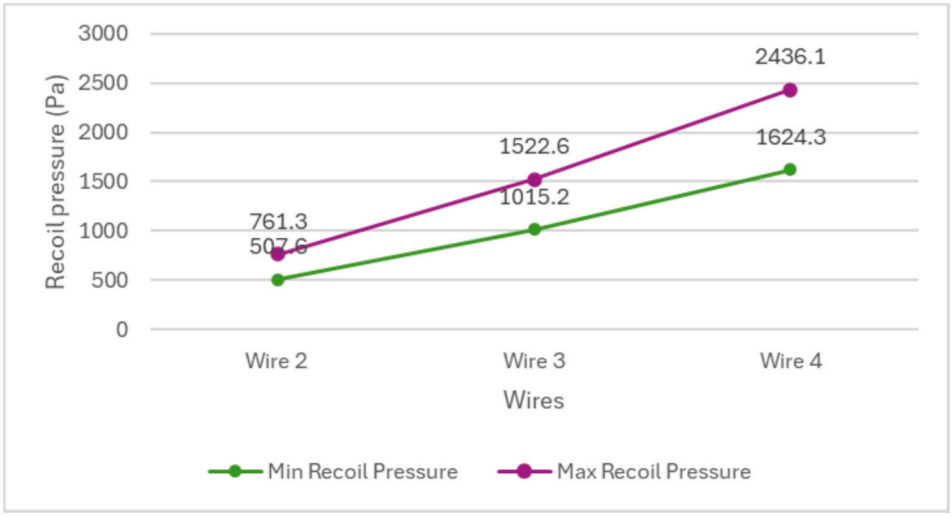

Fig. 24. The minimum and maximum recoil pressures acting on droplets as a function of sodium content.

Tashiro: Writing – review & editing, Supervision, Project administration, Funding acquisition, Conceptualization. **Quang Ngoc Trinh:** Methodology. **Tetsuo Suga:** Supervision. **Naoki Sawamura:** Resources. **Kazuhiro Fukuda:** Resources. **Shuji Sasakura:** Resources. **J. Eduardo Alvarez-Rocha:** Writing – review & editing. **Patricio Fernando Mendez:** Writing – review & editing. **Anthony B. Murphy:** Writing – review & editing, Resources. **Van Hanh Bui:** Writing – review & editing. **Manabu Tanaka:** Writing – review & editing.

Declaration of competing interest

The authors declare that they have no known competing financial interests or personal relationships that could have appeared to influence the work reported in this paper.

Acknowledgement

This work was supported by JSPS KAKENHI (Grant Number JP21K04710), the Project on Design & Engineering by Joint Inverse Innovation for Materials Architecture (DEJI2MA) from the Ministry of Education, Culture, Sports, Science and Technology (MEXT), and an OU Master Plan Implementation Project promoted under Osaka University.

References

[1] AWS. Welding handbook, chapter 5, flux cored arc weldingvol. 2, Part 1; 2004.
[2] Hadžihafizović D. Flux cored arc welding, Sarajevo. 2022.
[3] Świerczyńska Aleksandra, Varbai Balázs, Pandey Chandan, Fydrych Dariusz. Exploring the trends in flux-cored arc welding: scientometric analysis approach. The International Journal of Advanced Manufacturing Technology 2024;130:87–100.
[4] Yu Jiyoung, Cho Seung Mok. Metal-cored welding wire for minimizing weld porosity of zinc-coated steel. Journal of Materials Processing Tech 2017;249:350–7.
[5] French IE, Bosworth MR. A comparison of pulsed and conventional welding with basic flux cored and metal cored welding wires. Welding Research Supplement 1995:197s–205s.
[6] Bauné E, Bonnet C, Liu S. Assessing metal transfer stability and spatter severity in flux cored arc welding. Science and Technology of Welding and Joining 2001;6(3):139–48.
[7] Lu Fenggui, Wang Hui-Ping, Murphy Anthony B, Carlson Blair E. Analysis of energy flow in gas metal arc welding processes through self-consistent three-dimensional process simulation. International Journal of Heat and Mass Transfer 2014;68:215–23.
[8] K. M. S. a. P. M. E. J. Soderstrom. Calorimetric measurement of droplet temperature in GMAW. Welding Research 2011;90:77s–84s.
[9] Scotti Américo, Ponomarev Vladimir, Lucas William. A scientific application oriented classification for metal transfer modes in GMA welding. J Mater Process Technol 2012;212:1406–13.
[10] Paul Kah, Hamidreza Latifi, Raimo Suoranta, Jukka Martikainen, Markku Pirinen. Usability of arc types in industrial welding. International Journal of Mechanical and Materials Engineering 2014;9:15.
[11] Danut Iordachescu LQ. Steps toward a new classification of metal transfer in gas metal arc welding. J Mater Process Technol 2008;202:391–7.
[12] Lancaster JF. The physic of welding. Great Britain: A. Wheaton & Co. Ltd., Exeter; 1986.
[13] Ushio M, Ikeuchi K, Tanaka M, Seto T. Effects of shielding gas on metal transfer. Welding International 1995;9(6):462–6.
[14] Hertel M, Spille-Kohoff A, Füssel U, Schnick M. Numerical simulation of droplet detachment in pulsed gas–metal arc welding including the influence of metal vapour. J Phys D Appl Phys 2013;46:224003.
[15] Ogino Yosuke, Hirata Yoshinori, Asai Satoru. Discussion of the effect of shielding gas and conductivity of vapor core on metal transfer phenomena in gas metal arc welding by numerical simulation. Plasma Chemistry and Plasma Processing 2020;40:1109–26.
[16] Liu S, Siewert TA. Metal transfer in gas metal arc welding: droplet rate. Welding Research Supplement 1989:52s–8s.
[17] Hu J, Tsai HL. Heat and mass transfer in gas metal arc welding. Part II: the metal. International Journal of Heat and Mass Transfer 2007;50:808–20.
[18] Kim Y-S, Eagar TW. Analysis of metal transfer in gas metal arc welding. Welding Research Supplement 1993:269s–78s.
[19] Starling CMD, Modenesi PJ. Metal transfer evaluation of tubular wires. Welding International 2007;21(6):412–20.
[20] Trinh Ngoc Quang, Tashiro Shinichi, Le Khoi Dang, Suga Tetsuo, Kakizaki Tomonori, Yamazaki Kei, et al. Eligible CO2 content in Ar-CO2 mixture shielding gas for improving metal transfer in metal-cored arc welding. International Journal of Heat and Mass Transfer 2024;231:125803.
[21] Tashiro Shinichi, Trinh Quang Ngoc, Le Dang Khoi, Suga Tetsuo, Kakizaki Tomonori, Yamazaki Kei, et al. Elucidation of droplet detachment mechanism in metal-cored arc welding. Journal of Manufacturing Processes 2024;124:1583–605.
[22] Valensi F, Pellerin N, Pellerin S, Castillon Q, Dzierzega K, Briand F, et al. Influence of wire initial composition on anode microstructure and on metal transfer mode in GMAW: noteworthy role of alkali elements. Plasma Chem Plasma Process 2018;38:177–205.
[23] Trinh Ngoc Quang, Tashiro Shinichi, Tanaka Keigo, Suga Tetsuo, Kakizaki Tomonori, Yamazaki Kei, et al. Effects of alkaline elements on the metal transfer behavior in metal cored arc welding. Journal of Manufacturing Processes 2021;68:1448–57.
[24] Van Bui Hanh, Trinh Ngoc Quang, Tashiro Shinichi, Suga Tetsuo, Kakizaki Tomonori, Yamazaki Kei, et al. Individual effects of alkali element and wire structure on metal transfer process in argon metal-cored arc welding. Materials 2023;16:3053.
[25] Kordi Hamed Alinezhad, Ghasempour-Mouziraji Mehran, Hosseinzadeh Morteza. Metal transfer mapping for flux-cored arc welding process by using near-infrared filming. Journal of Materials Engineering and Performance 2021;30:3079–95.
[26] Izutani Shun, Shimizu Hiroyuki, Suzuki Keiichi, Koshiishi Fusaki, Hirata Yoshinori. Observation and classification of droplet transfer in gas metal arc welding. In: IIW commission XII; 2006.
[27] Matsuda Fukuhisa, Ushio Masao, Tsuji Tatsuo, Mizuta Toshihiko. Arc characteristics and metal transfer for flux- cored electrode in GMA welding (report II). Transactions of JWRI 1980;9(1):39–46.
[28] Trinh Ngoc Quang, Le Khoi Dang, Tashiro Shinichi, Suga Tetsuo, Sasakura Shuji, Fukuda Kazuhiro, et al. Optimization of metal transfer in rutile flux-cored arc welding through controlled CO2 concentration in argon–CO2 shielding gas. Journal of Manufacturing Processes 2024;124:590–603.

[29] Suga Tetsuo, Kobayashi Minoru. Droplet transfer phenomena in CO2 arc welding by flux-cored wire. Proceedings of the Japan Welding Society 1985;3:269–75.
[30] Methong Titinan, Yamaguchi Tasuku, Shigeta Masaya, Tanaka Manabu, Ikeda Rinsei, Matsushita Muneo, et al. Effect of rare earth metal on plasma properties in GMAW using CO2 shielding gas. Weld World 2017;61:1039–47.
[31] Ogino Yosuke, Hirata Yoshinori. Numerical simulation of GMA metal transfer phenomena including arc plasma. Proceedings of the Japan Welding Society 2015; 33:1–12.
[32] Martin von Allmen AB. Laser-beam interactions with materials. Springer; 1995.
[33] Murphy AB, Arundell CJ. Transport coeficients of argon, nitrogen, oxygen, argon-nitrogen and argon-oxygen plasma. Plasma Chem. Plasma Process 1994;14: 451–90.
[34] Murphy A. Transport coefficients of air, argon-air, nitrogen-air, and oxygen-air plasma. Plasma Chem Plasma Process 1995;15:279–307.
[35] Murphy A. The effects of metal vapor in arc welding. J Phys D Appl Phys 2010;43: 434001.
[36] Capitelli M, Cappelletti D, Colonna G, Gorse C, Laricchiuta A, Liuti G, et al. On the possibility of using model potentials for collision integral calculations of interest for planetary atmospheres. Chem Phys 2007;338:62–6.
[37] Cambi R, Cappelletti D, Liuti G, Pirani F. Generalized correlations in terms of polarizability for van der Waals interaction potential parameter calculations. J Chem Phys 1991;95:1852–61.
[38] Sakabe S, Izawa Y. Cross sections for resonat charge transfer between atoms and their possitive ions: collision velocity < 1 a.u. Atom Data Nucl Data Tab 1991;49: 257–314.
[39] Nakamura Y, Lucas J. Electron drift velocity and momentum cross-section in mercury, sodium and thallium vapours: II: theoretical. J Phys D Appl Phys 1978; 11:337–45.
[40] Tanaka M, Yamamoto K, Tashiro S, Nakata K, Yamamoto E, Yamazaki K, et al. Time-dependent calculations of molten pool formation and thermal plasma with metal vapour in gas tungsten arc welding. J Phys D Appl Phys 2010;43:434009.
[41] Mcintosh C, Chapuis J, Mendez P. Effect of Ar-CO2 gas blends on droplet temperature in GMAW. Supplement to the Welding Journal 2016;95:273s–9s.
[42] Ogino Yosuke, Hirata Yoshinori, Murphy Anthony B. Numerical simulation ofGMAWprocess using Ar and an Ar–CO2 gas mixture. Weld World 2016;60: 345–53.